Noname manuscript No.
(will be inserted by the editor)

On a spatial-temporal decomposition of the optical flow

Aniello Raffaele Patrone · Otmar Scherzer

Received: date / Accepted: date

Abstract In this paper we present the first variational spatial-temporal decomposition algorithm for computation of the optical flow of a dynamic sequence. We consider several applications, such as the extraction of temporal motion patterns of different scales and motion detection in dynamic sequences under varying illumination conditions, such as they appear for instance in psychological flickering experiments. In order to take into account variable illumination conditions we review the derivation, and modify, the optical flow equation. Concerning the numerical implementation, we propose a relaxation approach for the adapted model such that the resulting optimality condition is an *integro-differential* equation, which is numerically solved by a fixed point iteration. For comparison purposes we use the standard time dependent optical flow algorithm from Weickert-Schnörr, which in contrast to our method, constitutes in solving a spatial-temporal *differential* equation.

Analysing the motion in a dynamic sequence is of interest in many fields of applications, like human computer interaction, medical imaging, psychology, to mention but a few.

In this paper we study the extraction of motion in dynamic sequences by means of the optical flow, which is the apparent motion of objects, surfaces, and edges in a dynamic visual scene caused by the relative motion between an observer and the scene.

Aniello Raffaele Patrone
Computational Science Center
University of Vienna
Oskar-Morgenstern Platz 1, 1090 Vienna, Austria
E-mail: aniello.patrone@univie.ac.at

Otmar Scherzer
Computational Science Center
University of Vienna
Oskar-Morgenstern Platz 1, 1090 Vienna, Austria
and
Johann Radon Institute for Computational and Applied Mathematics (RICAM)
Altenbergerstraße 69, 4040 Linz, Austria
E-mail: otmar.scherzer@univie.ac.at

There have been proposed several computational approaches for optical flow computations in the literature. In this paper we emphasize on variational methods. In this research area the first method is due to Horn & Schunck (Horn and Schunck, 1981). The method analyses two consecutive frames of the dynamic sequences. Several alternatives and generalizations have been proposed in the literature which are based on the paradigm of analysing two consecutive frames. Due to the huge amount of literature in this field we cannot provide a complete list of references and thus it is omitted at this point.

Relevant for this work is that we consider a dynamic sequence where all available frames are taken into account at once in the optical flow computations. We also formulate the variational optical flow problem in an infinite dimensional function space setting. Spatial-temporal optical flow methods in an infinite dimensional framework as the basis of numerical algorithms were previously studied by Weickert & Schnörr (Weickert and Schnörr, 2001a,b), (Borzi et al, 2002), (Wang et al, 2008) and (Andreev et al, 2015). The Weickert & Schnörr algorithm serves as a reference method for comparison with our algorithm. However, we mention that our prime objective is different than in (Weickert and Schnörr, 2001a,b), and consists in determining only selected flow components (instead of the whole flow as in (Weickert and Schnörr, 2001a,b)), and thus the comparison can never be fair.

In this paper we emphasize on the decomposition of the optical flow into several components. Here, we are implementing similar ideas as have been used before for variational image denoising (Vese and Osher, 2004; Aubert and Aujol, 2005; Aujol et al, 2005; Aujol and Chambolle, 2005; Aujol et al, 2006; Aujol and Kang, 2006; Duval et al, 2010). Image decomposition has been carried over to optical flow decomposition (Kohlberger et al, 2003; Yuan et al, 2007, 2008, 2009; Abhau et al, 2009). The context of the present paper, however, is different, because here we aim for extracting temporal patterns. We emphasize that the proposed method is one of very few variational optical flow algorithms in a space-time regime. Within this class this algorithm it is the only spatial-temporal decomposition algorithm. Variational modelling of patterns, which has been initialized with the seminal book of Y. Meyer (Meyer, 2001). In the context of total variation regularization, reconstructions of patterns was studied in (Vese and Osher, 2003) for the first time. There, it has been shown that dual norms are capable of characterizing patterns, which has been utilized in many of the denoising papers mentioned above. As already mentioned above, we use these ideas in order to extract temporal patterns.

A further aspect of this paper concerns comments on the well-posedness and the modeling of optical flow equations in a space-time regime. In particular, we present two different kind of modeling, based on a free surface formulation in space-time, and a presmoothing approach, respectively. Both of these approaches are formulated in an time-continuous setting. A paradigm of test problems are flickering experiments, where in a dynamic sequence there is an abrupt illumination change at a certain time frame. In our experiments, the perturbation concerns, for test cases, a whole image frame and can be determined a-priori, which does not need to be the case in general. This is useful for evaluating our experimental results in a controlled environment. In the context of registration illumination changes have been taken into account by (Miller and Younes, 2001) assuming smooth images. Recently, in (Berkels et al, 2015) they consider non-smooth images and transitions - this field is now denoted by Metamorphosis. (Miller and Younes, 2001; Berkels et al, 2015) have implemented models of mass conservation equations, as we did for optical flow computations in (Andreev et al, 2015). Nevertheless, the model we are choosing is based on a optical flow equation. In our example we assume illumination changes, which influence the mean intensities of the frames. As we show below such variations appear mathematically in any image sequence due to aggregations of characteristics. Therefore, we propose to constrain the space-time domain locally. This will result in local flow fields, which determine the optical flow.

For the numerical realization, we propose a relaxation approach, which consists in solving the optical flow minimization problem without taking into account brightness illumination changes.

The outline of this paper is as follows: In Section 1 we review the optical flow equation. In Section 3 and 4 we introduce the new model on spatial-temporal optical flow decomposition. We formulate it as a minimization problem and obtain the optimality conditions for a minimizer. In Section 5 we make calculations, which help to understand the decomposition algorithm from an analytical point of view. In Section 6 we derive a fixed point algorithm for numerical minimization of the energy functional. Finally in Section 8 and Section 9 we present experiments, results and a discussion of them.

1 Registration and optical flow

The problem of aligning dynamic sequences $f(\cdot, t)$ can be formulated as the operator equation, of finding a flow Ψ of diffeomorphisms,

$$\Psi(t) : \Omega \to \Omega\,, \quad \forall t \in [0, T]\,,$$

such that

$$f(\Psi(\mathbf{x}, t), t) = f(\mathbf{x}, 0)\,, \qquad \forall t \in [0, T]\,. \tag{1}$$

For natural images, in general, it is not possible to solve equation (1) subject to the constraint that Ψ is a diffeomorphism for every t, because of occlusions, illumination changes, noise, and information gain/loss in the movie over time. Thus the optical flow and image registration community typically do not consider this constraint, in contrast to the shape registration community (see for instance (Bauer et al, 2014; Jain et al, 2013)).

Differentiation of (1) with respect to t for a fixed $\mathbf{x}$ gives

$$\begin{aligned} &\nabla f(\Psi(\mathbf{x}, t), t) \cdot \partial_t \Psi(\mathbf{x}, t) + \partial_t f(\Psi(\mathbf{x}, t), t) = 0\,, \\ &\quad \forall t \in [T^l_{\mathbf{x}}, T^u_{\mathbf{x}}]\,. \end{aligned} \tag{2}$$

This equation only holds locally in time for points $\Psi(\mathbf{x}, t)$. For fixed $t > 0$, $\Psi(., t)$ is not a diffeomorphism on Ω, and therefore it does not cover the whole domain Ω. This is one of the reasons, while a least-squares approach is preferable against the *optical flow equation (OFE)* over all Ω (the characteristic equations starting from time $t = 0$ do not cover Ω completely:

$$\begin{aligned} &\nabla f(\mathbf{x}, t) \cdot \mathbf{u}(\mathbf{x}, t) + \partial_t f(\mathbf{x}, t) = 0\,, \\ &\quad \forall \mathbf{x} \in \Omega \text{ and } t \in [0, T]\,, \end{aligned} \tag{3}$$

where $\mathbf{u} = \partial_t \Psi$. That is, the problem is relaxed to calculate a minimizer of the functional

$$S(\mathbf{u}) = \int_\Omega (\nabla f(\mathbf{x},t) \cdot \mathbf{u}(\mathbf{x},t) + \partial_t f(\mathbf{x},t))^2 \, \mathrm{d}\mathbf{x} \to \min \,, \tag{4}$$

subject to some constraints.

Remark 1 We summarize the statements above and support it by some additional arguments: The optical flow equation is a realization of the brightness constancy assumption in a domain covered by the characteristics. This means that (3) is not well-motivated on subsets of Ω which are not met by a characteristic curve in space and time starting from $t = 0$. The situation is less relevant if the optical flow equation is considered for just two consecutive frames, which is the standard optical flow approach in the literature, because through the re-initialization at each pair of frame always a characteristic originates at some point Ω.

Let us assume that the domain Ω is completely covered by points on characteristic curves at a certain time t (meaning that $\Psi(t)$ is a diffeomorphism), then this would mean that flow and image sequence are trivial, as can be seen as follows: Constant brightness and full coverage by characteristics at some time T means that optical flow equation and the scalar transport equation, describing preservation of intensity,

$$\partial_t f + \nabla \cdot (f\mathbf{u}) = 0 \text{ in } \Omega \times [0,T] \,, \tag{5}$$

hold, respectively (see (Andreev et al, 2015)). Then, the optical flow equation provides that

$$f \nabla \cdot \mathbf{u} = 0 \text{ in } \Omega \times [0,T] \,. \tag{6}$$

This means that either $f = 0$ or $\mathbf{u}$ is divergence free. The solution of this equation is given by $\mathbf{u} \equiv 0$, which is the one with minimal energy $\mathcal{R}(\mathbf{u})$, if $\mathcal{R}(\mathbf{u}) \geq 0$ and $\mathcal{R}(\mathbf{u}) = 0$ iff $\mathbf{u} = 0$. Thus the solution is trivial.

The optical flow equation is linear, and satisfies the constant brightness assumption along the characteristics. The basic philosophy of this paper is to reconsider the optical flow equation in subdomains of the space-time domain where the characteristic equation is valid. In the subdomains we consider the standard optical flow equation. Thus methodological we can deal for instance with sudden intensity changes, which might appear locally or globally. Such changes could be for instance occlusions, illumination changes, flickering. Aside from theoretical challenges on this problem the numerical solution is challenging. Below, we discuss two options (by exclusion of singularities of the characteristics and by pre-smoothing of the data) of reformulating the optical flow equation in a space-time regime for consistent registration, which are the basis of numerical realization. Hard - and soft- flickering examples are considered as test examples for the different cases. We emphasize that in the crass flickering experiment, of course, we could determine the flickering frames a-priori. However, we want to do a blind implementation, without this pre-processing. Flickering experiments are a perfect test-scenario in a controlled environment.

2 The optical flow equation in case of illumination disturbances

In this section we present simple examples showing that the optical flow equation (3) is only locally coherent with the nonlinear registration equation (1). Moreover, we compare in a simple example the effect of sudden illumination changes and pre-smoothing of the data variants, which is a common technique in optical flow problems in spatial domain. Here, however, it is in spatial-temporal domain.

Example 1 In flickering experiments probands are exposed to a movie, consisting of slightly changing frames containing a significant disturbance, which could be a whole frame, or a series of frames. In general, the probands do not get conscious of the perturbation but are able to better focus on small variations in the remaining movie.

Hard flickering experiment: We motivate the consequences on deformation mappings and optical flow computations by some toy example: Let the movie sequence

$$\left\{ f(x,t) = \chi_{[\frac{1}{2},1]}(t)\chi_{[\frac{1}{2},1]}(x) : t \in [0,1] \right\} ,$$

be given, where χ is a characteristic function. Several deformations can be considered. The most intuitive one is:

$$\begin{aligned} \Psi(x,t) &= x\,, \qquad \forall t \in [0,1], x \in [0,0.5)\,, \\ \Psi(x,t) &= \begin{cases} x & \forall t \in [0,0.5), x \in [0.5,1)\,, \\ x & \forall t \in (0.5,1], x \in [0.5,1)\,, \end{cases} \end{aligned} \tag{7}$$

The deformation paths locally satisfy the nonlinear optical flow equation (2). In this case $u = \psi_t = 0$ almost everywhere.

A different deformation satisfying (2) is

$$\begin{aligned} \Psi(x,t) &:= \Psi\left(\frac{x}{1-t}, 0\right) := \frac{x}{1-t}\,, \\ &\qquad t \in [0,1/2], x \in [0,1-t]\,, \\ \Psi(x,t) &:= x\,, \quad t \in (1/2,1]\,, \\ u &= \Psi_t = \frac{x}{(1-t)^2}\,. \end{aligned} \tag{8}$$

Both deformations Ψ are injective for all $t \in [0,1]$ and along each path they are even differentiable almost everywhere. Because the range of Ψ is not the complete $\Omega \times [0,1]$, paths can be added artificially.

For this example we propose the following formulation of the optical flow equation: Let

$$\begin{aligned} \mathcal{D} &= \left\{ (x,t) \in [0,1]^2 : f \text{ is discontinuous at } (x,t) \right\} \\ &= [0.5,1] \times \{0.5\} \cup \{0.5\} \times [0.5,1]\,. \end{aligned}$$

denote the *discontinuity set* of f. Then, the proposed formulation of optical flow equation (3) is

$$\partial_x f(x,t) u(x,t) + \partial_t f(x,t) = 0\,, \qquad \forall (x,t) \notin \mathcal{D}\,, \tag{9}$$

with $u(x,t) = \partial_t \Psi(x,t)$.

In the following we assume that discontinuities of f only appear in t-direction at $S = \{t_0, t_1, \cdots, t_n\}$. Therefore, the discontinuity set of f is given by

$$\mathcal{D} = \{(x,t) : t \in S \text{ and } x \in \Omega\} \ .$$

As a consequence, variational optical flow methods consist in minimization of functionals

$$u \to \int_{\Omega \times [0,T] \setminus S} (\partial_x f(x,t) u(x,t) + \partial_t f(x,t))^2 \mathrm{d}x\mathrm{d}t + \alpha \mathcal{R}(u)\,,$$

where we assume that $\mathcal{R}$ is strictly convex and $\mathcal{R}(u) = 0$ if and only if $u \equiv 0$. To be consistent with the evaluation of $\partial_t f$, it has to be computed with an *up-wind scheme*:

$$\partial_t f \approx \begin{cases} \frac{f_i^{n+1} - f_i^n}{\Delta t} & \text{if } \left|f_i^{n+1} - f_i^n\right| < \left|f_i^n - f_i^{n-1}\right| \,, \\ \frac{f_i^n - f_i^{n-1}}{\Delta t} & \text{else} \end{cases}$$

where

$$f_i^n \approx f(x_i, t_n) \ .$$

where x_i denotes the spatial information of the generic pixel i at time level t_n. With this scheme it is inherent that we get the intuitive deformation $\Psi(x,t) = x$ (cf. (7)). That is $u = 0$.

In the following we analyse the appearance of singularities of the optical flow and the characteristics.

Example 2 A soft flickering example: In contrast to hard flickering, soft flickering interpolates between frames and perturbations. The flow behaves significantly different, as we see below.

We consider the one dimensional optical flow problem, to solve for u in

$$\partial_x f(x,t) u(x,t) + \partial_t f(x,t) = 0 \text{ in } (0,1) \times (0,1) \tag{10}$$

for the specific test data

$$f(x,t) = \tilde{f}(x) g(t) \text{ for } (x,t) \in (0,1) \times (0,1) \ . \tag{11}$$

f denotes a dynamic sequence with brightness variation over time and $\partial_x f(x,t)$, $\partial_t f(x,t)$ are its partial derivatives over space and time, respectively.

We take specifically:

$$\tilde{f}(x) = x(1-x) \text{ and } g(t) = 1 - t \ . \tag{12}$$

This is a sort of soft flickering experiment with a smooth transition of appearance. The resulting function f and the level lines are plotted in Figure 1, 2.

In this case we have $\partial_x \tilde{f}(x) = 1 - 2x$, and thus

$$u(x,t) = \frac{x(1-x)}{1-2x} \frac{1}{1-t}\,,$$

The optical flow u indicates that the transport of intensities is from left to right on the left side of $1/2$ and opposite on the other, which is an effect of the loss of intensities at $x = 1/2$. We observe that $u(0.5,t)$, $u(x,1)$ are singularities of the characteristics.

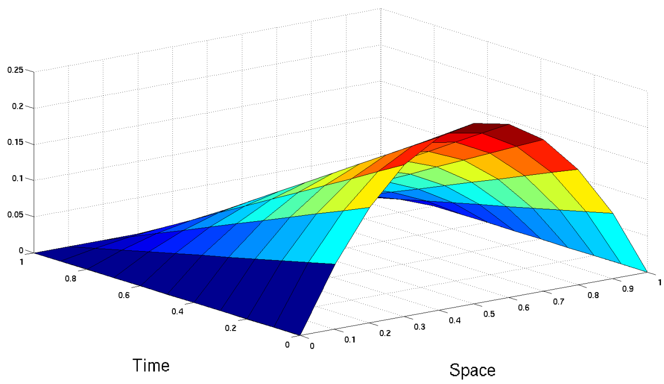

Fig. 1: $f(x,t) = (x(1-x)(1-t))$ from (12).

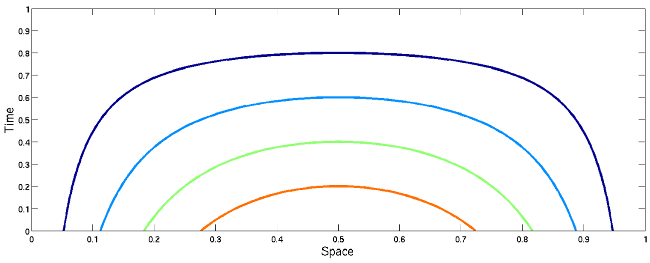

Fig. 2: Level lines Ψ of f. u approximates Ψ_t.

Moreover, we have

$$\int_0^t u(x,\tau)\,d\tau = -\frac{x(1-x)}{1-2x}\log(1-t)\ .$$

Thus

$$\begin{aligned}
&\left\| (x,t) \to \int_0^t u(x,\tau)\,d\tau \right\|^2_{L^2((0,1)^2)} \\
=&\int_0^1 \frac{x^2(1-x)^2}{(1-2x)^2}\,dx \int_0^1 \log^2(1-t)\,dt \\
=&\int_0^1 \frac{x^2(1-x)^2}{(1-2x)^2}\,dx \int_0^1 \log^2(t)\,dt \\
=&2\int_0^1 \frac{x^2(1-x)^2}{(1-2x)^2}\,dx \\
=&\infty\,,
\end{aligned}$$

which implies that

$$(x,t) \to \int_0^t u(x,\tau)\,d\tau \notin L^2((0,1)^2)\ .$$

Now, we calculate the actual deformations Ψ from the non-linear optical flow equation (2), which is

$$\Psi_t(x,t) = \frac{\Psi(x,t)(1-\Psi(x,t))}{1-2\Psi(x,t)} \frac{1}{1-t} \; . \tag{13}$$

We also have the initial condition

$$\Psi(x,0) = x \,, \quad \forall x \in (0,1) \; . \tag{14}$$

We make a separation of variables ansatz to solve the ordinary differential equation (ODE) (13), (14): Let

$$\begin{aligned}\rho(y) &:= \int_x^y \frac{1-2s}{s(1-s)}\, ds \\ &= \log(y(1-y)) - \log(x(1-x))\,,\end{aligned}$$

and take into account that

$$\int_0^t \frac{1}{1-t}\, dt \;= -\log(1-t) \; .$$

The separation of variables ansatz allows to determine the solution of the ODE as the solution of the equation

$$\rho(\Psi(x,t)) = -\log(1-t) \; .$$

Thus we get the solution of the characteristics of the registration problem:

$$\Psi(x,t) = \frac{1}{2} \pm \sqrt{\frac{1}{4} - \frac{x(1-x)}{1-t}} \text{ for } t \leq 4\left(x-\frac{1}{2}\right)^2 ,$$

where the branch of Ψ with $+$ is active if $x > 1/2$ and the other branch holds for $x < 1/2$. Moreover, we have

$$u_N(x,t) := \partial_t \Psi(x,t) = \mp \frac{x(1-x)}{\sqrt{1-t-4x(1-x)}} \frac{1}{(1-t)^{3/2}} \; .$$

This shows that the flow has a singularity (endpoint) at $t = 1-4x(1-x)$.

In Figure 3 there are shown u and u_N. Essentially this makes transparent the time interval in which the optical flow equation is valid. For a short time interval it very well aligns with the registration problem. Also this argument shows that different aspects have to be considered for standard (quasi-static) optical flow and time-continuous optical flow. For analysis of two consecutive frames this is not relevant.

Example 3 We consider again a simple example (11) but with

$$\tilde{f}(x) = \left(x - \frac{1}{2}\right)^2 \text{ and } g(t) = 1-t \; .$$

Then

$$u(x,t) = \frac{\left(x-\frac{1}{2}\right)^2}{2x-1} \frac{1}{1-t} \; .$$

Again, $u(x,1)$ is singular. Note, however that

$$\int_0^t u(x,\tau)\, d\tau = -\frac{1}{4}(x^2-x)\log(1-t) \in L^2((0,1)^2) \; .$$

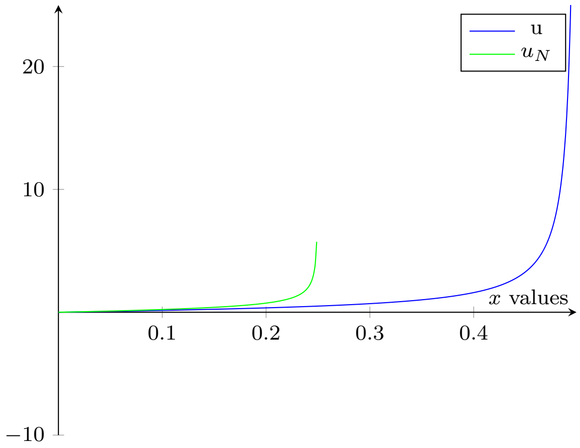

Fig. 3: Linear versus non-linear optical flow: u and u_N at $t = 1/4$. Note that u_N is only defined in the interval $[0, 1/4]$, which is plotted, while u is defined for $[0, 1/2)$.

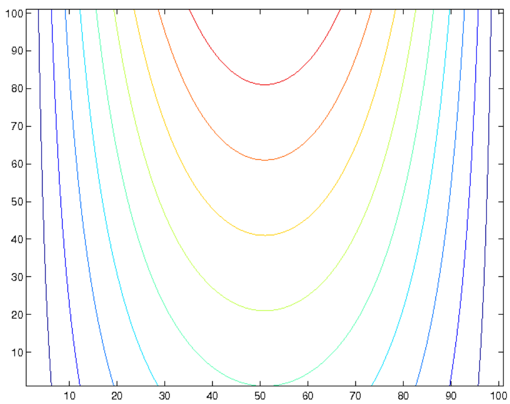

Fig. 4: Level lines Ψ of f. u approximates Ψ_t.

Example 4 If instead of interpolating $x \to x(1-x)$ and $x \to 0$ as in Example (2), one interpolates $x \to x(1-x)$ and $x \to 2x(1-x)$. That is

$$f(x,t) = x(1-x)(1+t) \ .$$

In Figure 4 are reported the level lines of f. Then the singularity of u at time 1 of the previous example is not present, and

$$u(x,t) = \frac{\left(x - \frac{1}{2}\right)^2}{2x-1}\frac{1}{1+t} \ .$$

We emphasize here that brightness constancy does not hold globally - there is obviously a global illumination change over time. Intensity values can be registered over time for every spatial point except at $x = 1/2$. The characteristics of (2) are well-defined for limited time-spans, depending on the location distance to $x = 1/2$.

This shows that on the sets $\{(x,t) : x > 1/2, t < 1\}$ and $\{(x,t) : x < 1/2, t < 1\}$ the optical flow equation holds. We clarify that the characteristics have a singularity at $x = 1/2$.

The bottom line of these examples is that illumination changes, such as flickering, may result in singularities of the characteristics of the registration problem or the optical flow field. Singularities in the space variable might also appear, but they are neglected here. The potential appearance of the singularity in time motivates us to consider regularization terms for optical flow computations, which allow for singularities over time, such as negative Sobolev norms or G-norms.

3 Optical flow decomposition: basic setup and formalism

In this paper we derive an optical flow model that allows to decompose the flow field into spatial and temporal components.

The *standard optical flow* (Horn and Schunck, 1981) is a vector field

$$\mathbf{u} = \begin{pmatrix} u_1 \\ u_2 \end{pmatrix} : \Omega \times (0,1) \to \mathbb{R}^2 ,$$

connecting an image sequence

$$f : \Omega \times (0,1) \to \mathbb{R} .$$

We always assume that the image sequence is scaled to the time-interval $(0,1)$ and $\Omega = (0,1)$.

In this paper we consider the optical flow field

$$\mathbf{u}(\mathbf{x},t) = \mathbf{u}^{(1)}(\mathbf{x},t) + \mathbf{u}^{(2)}(\mathbf{x},t)$$

as a compound of two flow field components

$$\mathbf{u}^{(1)}(\mathbf{x},t) = \begin{pmatrix} u_1^{(1)}(\mathbf{x},t) \\ u_2^{(1)}(\mathbf{x},t) \end{pmatrix} , \quad \mathbf{u}^{(2)}(\mathbf{x},t) = \begin{pmatrix} u_1^{(2)}(\mathbf{x},t) \\ u_2^{(2)}(\mathbf{x},t) \end{pmatrix} .$$

Because there is a series of indices and variables it is appropriate to specify the notation at this point:

$\mathbf{x} = (x_1, x_2)$	Euclidean space
$\partial_k = \frac{\partial}{\partial x_k}$	Differentiation with respect to spatial variable x_k
$\partial_t = \frac{\partial}{\partial t}$	Differentiation with respect to time
$\nabla = (\partial_1, \partial_2)^T$	Gradient in space
$\nabla_3 = (\partial_1, \partial_2, \partial_t)^T$	Gradient in space and time
$\nabla \cdot = \partial_1 + \partial_2$	Divergence in space
$\nabla_3 \cdot = \partial_1 + \partial_2 + \partial_t$	Divergence in space and time
$\Delta = \partial_1^2 + \partial_2^2$	2-dimensional Laplace
$\mathbf{n}$	normal vector to Ω
f	input sequence
$f(\cdot, t)$	movie frame
$\mathbf{u}^{(i)}$	optical flow module, $i = 1, 2$
$\mathbf{u} = \mathbf{u}^{(1)} + \mathbf{u}^{(2)}$	optical flow module, $i = 1, 2$
$u_j^{(i)}$	j-th optical flow component of the i-th module
$\psi^{(i)}$ satisfying $\partial_t \psi^{(i)}(\mathbf{x}, t) = \mathbf{u}^{(i)}(\mathbf{x}, t)$	variation of deformation, $i = 1, 2$
$\psi = \psi^{(1)} + \psi^{(2)}$	total variation of deformation
$\Psi^{(i)}(\mathbf{x}, t) = \mathbf{x} + \psi^{(i)}(\mathbf{x}, t)$	deformation
$\Psi = \Psi^{(1)} + \Psi^{(2)}$	total deformation

4 Variational methods for decomposition of the optical flow

In the setting of Section 4, the OFE-equation (3) contains four unknown (real valued) functions $u_j^{(i)}$, $i, j = 1, 2$, and thus is highly underdetermined.
To overcome the lack of equations, the problem is formulated as a constrained optimization problem:
Determine, for some fixed $\alpha > 0$,

$$\operatorname{argmin} \left(\mathcal{R}^{(1)}(\mathbf{u}^{(1)}) + \alpha \mathcal{R}^{(2)}(\mathbf{u}^{(2)}) \right) \tag{15}$$

subject to (3). Here $\mathcal{R}^{(i)}$, $i = 1, 2$ are convex functionals, such that $\mathcal{R}^{(1)} + \alpha \mathcal{R}^{(2)}$ is strictly convex. Instead of solving the constrained optimization problem, we use a soft variant and minimize the unconstrained regularization functional:

$$\begin{aligned} &\mathcal{F}(\mathbf{u}^{(1)}, \mathbf{u}^{(2)}) := \mathcal{E}(\mathbf{u}^{(1)}, \mathbf{u}^{(2)}) + \sum_{i=1}^{2} \alpha^{(i)} \mathcal{R}^{(i)}(\mathbf{u}^{(i)}) \,, \\ &\mathcal{E}(\mathbf{u}^{(1)}, \mathbf{u}^{(2)}) := \\ &\qquad \int_{\Omega \times (0,1)} (\nabla f \cdot (\mathbf{u}^{(1)} + \mathbf{u}^{(2)}) + \partial_t f)^2 \mathrm{d}\mathbf{x}\mathrm{d}t \,. \end{aligned} \tag{16}$$

Here

$$\alpha \approx \frac{\alpha^{(2)}}{\alpha^{(1)}} \,.$$

In the following we design the regularizers $\mathcal{R}^{(i)}$. Moreover, for the sake of simplicity of presentation, we omit the space and time arguments of the functions $u_j^{(i)}$ and f, whenever it simplifies the formulas.

- For $\mathcal{R}^{(1)}$ we use a common spatial-temporal regularization functional for optical flow regularization (see for instance (Weickert and Schnörr, 2001b)):

$$\begin{aligned} &\mathcal{R}^{(1)}(\mathbf{u}^{(1)}) \\ &:= \int_{\Omega\times(0,1)} \psi\left(\left|\nabla_3 u_1^{(1)}\right|^2 + \left|\nabla_3 u_2^{(1)}\right|^2\right) \mathrm{d}\mathbf{x}\mathrm{d}\tau\,, \end{aligned} \tag{17}$$

  where $\psi : \mathbb{R}_0^+ \to \mathbb{R}_0^+$ is a monotonically increasing, differentiable function. For the choice of ψ we follow (Weickert and Schnörr, 2001b):

$$\psi(r^2) = \epsilon r^2 + (1-\epsilon)\lambda^2\sqrt{1+\frac{r^2}{\lambda^2}} \tag{18}$$

  with $0 < \epsilon \ll 1$ and $\lambda > 0$. This function is convex in r and there exist constants $c_1, c_2 > 0$ with $c_1 r^2 \leq \psi(r^2) \leq c_2 r^2$ for all $r \in \mathbb{R}$.
- $\mathcal{R}^{(2)}$ is designed to penalize for variations of the second component in time. Motivated by Y. Meyer's book (Meyer, 2001), we introduce a regularization term, which is non-local in time. Moreover, this term is designed to be able to handle flickering experiments. In (Meyer, 2001) it was pointed out that the G-norm can be used to extract oscillations in images and the same feature was also exploited to extract patterns in the optical flow (Abhau et al, 2009). However, in all these works, spatial patterns were extracted. Here we emphasize on temporal patterns.
  It is a challenge to compute the G-norm efficiently, and therefore workarounds have been proposed. For instance (Vese and Osher, 2003) proposed as an alternative at the G-norm the following realization for the H^{-1} norm: For a generalized function $u : \Omega \to \mathbb{R}$, they defined

$$\|u\|_{H^{-1}}^2 = -\int_\Omega u(\mathbf{x})\Delta^{-1}u(\mathbf{x})d\mathbf{x}\,.$$

  Here, we use an analogous workaround as in (Vese and Osher, 2003) for a realization for the *temporal* H^{-1}-norm, and introduce the regularization functional:

$$\begin{aligned} \mathcal{R}^{(2)}(\mathbf{u}^{(2)}) &:= \int_{\Omega\times(0,1)} \left|\int_0^t \mathbf{u}^{(2)}(\mathbf{x},\tau)\mathrm{d}\tau\right|^2 \mathrm{d}\mathbf{x}\mathrm{d}t \\ &= \sum_{j=1}^2 \int_{\Omega\times(0,1)} \left(\int_0^t u_j^{(2)}(\mathbf{x},\tau)\mathrm{d}\tau\right)^2 \mathrm{d}\mathbf{x}\mathrm{d}t\,. \end{aligned} \tag{19}$$

  To see the analogy with the $\|\cdot\|_{H^{-1}}$-norm from (Vese and Osher, 2003) define the second primitive:

$$U_j^2(t) := -\int_t^1 \int_0^{\hat{t}} \mathbf{u}_j^{(2)}(\mathbf{x},\tau)\,\mathrm{d}\tau\mathrm{d}\hat{t}\,,$$

which corresponds to the inverse Laplacian in temporal domain. Then, from integration by parts it follows that

$$-\int_0^1 U_j^2(t) u_j^{(2)}(t)\,dt = \int_0^1 \int_0^t u_j^{(2)}(\tau)\mathrm{d}\tau \int_0^t u_j^{(2)}(\tau)\mathrm{d}\tau\,dt\;.$$

and therefore

$$\begin{aligned}\mathcal{R}^{(2)}(\mathbf{u}^{(2)}) &= \int_{\Omega\times(0,1)} U_j^{(2)}(\mathbf{x},t)\mathbf{u}_j^{(2)}(\mathbf{x},t)\mathrm{d}\mathbf{x}\mathrm{d}t \\ &= \sum_{j=1}^{2} \int_{\Omega} \left\| u_j^{(2)}(\mathbf{x},\cdot)\right\|_{H^{-1}}^2 \;.\end{aligned} \tag{20}$$

Even more, note that $\mathcal{R}^{(2)}$ penalizes the deformation, which is approximating the anti-derivative of the flow $\mathbf{u}$, with respect to time.

4.1 Energy functional and minimization

In this section we determine the optimality conditions for minimizers of $\mathcal{F}$ introduced in (16). Necessary conditions for a minimizer are that the directional derivatives vanish for all 2-dimensional vector valued functions $\mathbf{h}^{(i)}$, $i = 1, 2$. This means that

$$\begin{aligned}\lim_{s\to 0} \frac{\mathcal{F}(\mathbf{u}^{(1)} + s\mathbf{h}^{(1)}, \mathbf{u}^{(2)}) - \mathcal{F}(\mathbf{u}^{(1)}, \mathbf{u}^{(2)})}{s} &= 0\,,\\ \lim_{s\to 0} \frac{\mathcal{F}(\mathbf{u}^{(1)}, \mathbf{u}^{(2)} + s\mathbf{h}^{(2)}) - \mathcal{F}(\mathbf{u}^{(1)}, \mathbf{u}^{(2)})}{s} &= 0\end{aligned}$$

for all vector valued functions $\mathbf{h}^{(i)} : \Omega \times (0, 1) \to \mathbb{R}^2$. Because

$$\mathcal{F}(\mathbf{u}^{(1)}, \mathbf{u}^{(2)}) = \mathcal{E}(\mathbf{u}^{(1)}, \mathbf{u}^{(2)}) + \sum_{i=1}^{2} \alpha^{(i)} \mathcal{R}^{(i)}(\mathbf{u}^{(i)})\,,$$

it suffices to determine the directional derivatives of $\mathcal{F}$, $\mathcal{E}$ and $\mathcal{R}^{(i)}$, separately. The derivative of $\mathcal{E}$ is the weighted sum of the single components.

– The directional derivative of $\mathcal{R}^{(1)}$ at $\mathbf{u}^{(1)}$ in direction $\mathbf{h}^{(1)}$ is determined as follows: Let us abbreviate for simplicity of presentation

$$\begin{aligned}\psi &:= \psi\left(\left|\nabla_3 u_1^{(1)}\right|^2 + \left|\nabla_3 u_2^{(1)}\right|^2\right)\,,\\ \psi' &:= \psi'\left(\left|\nabla_3 u_1^{(1)}\right|^2 + \left|\nabla_3 u_2^{(1)}\right|^2\right)\,,\end{aligned}$$

then the directional derivative of $\mathcal{R}^{(1)}$ in direction $\mathbf{h}^{(1)}$ at $\mathbf{u}^{(1)}$ is given by

$$
\begin{aligned}
&\partial_{\mathbf{u}^{(1)}}\mathcal{R}^{(1)}(\mathbf{u}^{(1)})\mathbf{h}^{(1)} \\
&= \lim_{s\to 0} \frac{\mathcal{R}^{(1)}(\mathbf{u}^{(1)}+s\mathbf{h}^{(1)}) - \mathcal{R}^{(1)}(\mathbf{u}^{(1)})}{s} \\
&= \lim_{s\to 0} \frac{1}{s} \int_{\Omega\times(0,1)} \psi\left(\left|\nabla_3(u_1^{(1)}+sh_1^{(1)})\right|^2 \right. \\
&\qquad\qquad \left. + \left|\nabla_3(u_2^{(1)}+sh_2^{(1)})\right|^2 \right) - \psi \,\mathrm{d}\mathbf{x}\mathrm{d}t \\
&= -2 \int_{\Omega\times(0,1)} \nabla_3 \cdot \left(\psi' \nabla_3 u_1^{(1)}\right) h_1^{(1)} \\
&\qquad\qquad + \nabla_3 \cdot \left(\psi' \nabla_3 u_2^{(1)}\right) h_2^{(1)} \mathrm{d}\mathbf{x}\mathrm{d}t \,.
\end{aligned}
\tag{21}
$$

where integration by parts is used in the final step of the above derivation.

- The directional derivative of $\mathcal{E}$ in direction $\mathbf{h}^{(1)}$ is given by

$$
\begin{aligned}
&\partial_{\mathbf{u}^{(1)}}\mathcal{E}(\mathbf{u}^{(1)},\mathbf{u}^{(2)})\mathbf{h}^{(1)} \\
&= \lim_{s\to 0} \frac{\mathcal{E}(\mathbf{u}^{(1)}+s\mathbf{h}^{(1)},\mathbf{u}^{(2)}) - \mathcal{E}(\mathbf{u}^{(1)},\mathbf{u}^{(2)})}{s} \\
&=2 \int_{\Omega\times(0,1)} (\nabla f \cdot (\mathbf{u}^{(1)}+\mathbf{u}^{(2)}) + \partial_t f)(\nabla f \cdot \mathbf{h}^{(1)}) \,\mathrm{d}\mathbf{x}\mathrm{d}t \\
&=2 \int_{\Omega\times(0,1)} \nabla f(\nabla f \cdot (\mathbf{u}^{(1)}+\mathbf{u}^{(2)}) + \partial_t f) \cdot \mathbf{h}^{(1)} \,\mathrm{d}\mathbf{x}\mathrm{d}t \,.
\end{aligned}
\tag{22}
$$

- The derivative of $\mathcal{E}$ in the direction $\mathbf{h}^{(2)}$ is analogously derived:

$$
\begin{aligned}
&\partial_{\mathbf{u}^{(2)}}\mathcal{E}(\mathbf{u}^{(1)},\mathbf{u}^{(2)})\mathbf{h}^{(2)} \\
&= \lim_{s\to 0} \frac{\mathcal{E}(\mathbf{u}^{(1)},\mathbf{u}^{(2)}+s\mathbf{h}^{(2)}) - \mathcal{E}(\mathbf{u}^{(1)},\mathbf{u}^{(2)})}{s} \\
&=2 \int_{\Omega\times(0,1)} \nabla f(\nabla f \cdot (\mathbf{u}^{(1)}+\mathbf{u}^{(2)}) + \partial_t f) \cdot \mathbf{h}^{(2)} \,\mathrm{d}\mathbf{x}\mathrm{d}t \,.
\end{aligned}
\tag{23}
$$

- The directional derivative of $\mathcal{R}^{(2)}$ is derived as follows:

$$
\begin{aligned}
&\partial_{\mathbf{u}^{(2)}}\mathcal{R}^{(2)}(\mathbf{u}^{(2)})\mathbf{h}^{(2)} \\
&= \lim_{s\to 0} \frac{\mathcal{R}^{(2)}(\mathbf{u}^{(2)}+s\mathbf{h}^{(2)}) - \mathcal{R}^{(2)}(\mathbf{u}^{(2)})}{s} \\
&= \lim_{s\to 0} \frac{1}{s} \int_{\Omega\times(0,1)} \left(\left| \int_0^t \mathbf{u}^{(2)} + s\mathbf{h}^{(2)} \mathrm{d}\tau \right|^2 \right. \\
&\qquad\qquad \left. - \left| \int_0^t \mathbf{u}^{(2)} \mathrm{d}\tau \right|^2 \right) \mathrm{d}\mathbf{x}\mathrm{d}t \\
&=2 \sum_{j=1}^{2} \int_{\Omega\times(0,1)} \int_0^t u_j^{(2)} \mathrm{d}\tau \int_0^t h_j^{(2)} \mathrm{d}\tau \quad \mathrm{d}\mathbf{x}\mathrm{d}t \,.
\end{aligned}
\tag{24}
$$

Now, we denote by

$$U_j^{(2)}(\mathbf{x},t) := -\int_t^1 \int_0^\tau u_j^{(2)}(\mathbf{x},\tilde{\tau})\,\mathrm{d}\tilde{\tau}\mathrm{d}\tau \qquad \text{for } j=1,2 \tag{25}$$

the second primitive of the optical flow components.

From the definition (25) it follows that

$$\begin{aligned} U_j^{(2)}(\mathbf{x},1) &= 0 \text{ for } \mathbf{x}\in\Omega\,,\\ \partial_t U_j^{(2)}(\mathbf{x},0) &= \int_0^0 u_j^{(2)}(\mathbf{x},\tau)\,\mathrm{d}\tau = 0 \\ &\text{for } \mathbf{x}\in\Omega\,,\quad j=1,2\,. \end{aligned} \tag{26}$$

Moreover, it follows by integration by parts of the last line of (24) with respect to t that

$$\begin{aligned} &\partial_{\mathbf{u}^{(2)}}\mathcal{R}^{(2)}(\mathbf{u}^{(2)})\mathbf{h}^{(2)} = \\ &-2\sum_{j=1}^{2}\int_{\Omega\times(0,1)} U_j^{(2)}(\mathbf{x},t)h_j^{(2)}(\mathbf{x},t)\mathrm{d}\mathbf{x}\mathrm{d}t\,. \end{aligned} \tag{27}$$

The directional derivatives of $\mathcal{F}$ in directions $\mathbf{h}^{(1)}$ and $\mathbf{h}^{(2)}$ are given by

$$\begin{aligned} &\left(\partial_{\mathbf{u}^{(1)}}\mathcal{E}(\mathbf{u}^{(1)},\mathbf{u}^{(2)}) + \alpha^{(1)}\partial_{\mathbf{u}^{(1)}}\mathcal{R}^{(1)}(\mathbf{u}^{(1)})\right)\mathbf{h}^{(1)}\,,\\ &\left(\partial_{\mathbf{u}^{(2)}}\mathcal{E}(\mathbf{u}^{(1)},\mathbf{u}^{(2)}) + \alpha^{(2)}\partial_{\mathbf{u}^{(2)}}\mathcal{R}^{(2)}(\mathbf{u}^{(2)})\right)\mathbf{h}^{(2)}\,, \end{aligned}$$

respectively.

If $\mathbf{u}^{(1)},\mathbf{u}^{(2)}$ are the modules of a minimizer of $\mathcal{F}$, then for all vector valued functions $\mathbf{h}^{(1)}$, $\mathbf{h}^{(2)}$

$$\begin{aligned} 0 &= \left(\partial_{\mathbf{u}^{(1)}}\mathcal{E}(\mathbf{u}^{(1)},\mathbf{u}^{(2)}) + \alpha^{(1)}\partial_{\mathbf{u}^{(1)}}\mathcal{R}^{(1)}(\mathbf{u}^{(1)})\right)\mathbf{h}^{(1)}\,,\\ 0 &= \left(\partial_{\mathbf{u}^{(2)}}\mathcal{E}(\mathbf{u}^{(1)},\mathbf{u}^{(2)}) + \alpha^{(2)}\partial_{\mathbf{u}^{(2)}}\mathcal{R}^{(2)}(\mathbf{u}^{(2)})\right)\mathbf{h}^{(2)}\,. \end{aligned}$$

Now, because of (21) and (22) it follows that the minimizer $\mathbf{u}^{(i)}$, $i=1,2$ has to satisfy for every $j=1,2$,

$$\begin{aligned} &\partial_j f(\nabla f\cdot(\mathbf{u}^{(1)}+\mathbf{u}^{(2)})+\partial_t f)\\ &\quad-\alpha^{(1)}\nabla_3\cdot\left(\psi'\nabla_3 u_j^{(1)}\right) = 0 \text{ in } \Omega\times(0,1)\,,\\ &\frac{\partial u_j^{(1)}}{\partial\mathbf{n}} = 0 \text{ in } \partial\Omega\times(0,1)\,,\\ &\frac{\partial u_j^{(1)}}{\partial t} = 0 \text{ in } \Omega\times\{0,1\}\,. \end{aligned} \tag{28}$$

Because (27) holds for all $\mathbf{h}_j^{(2)}$, it follows from (23) and (27) that for every $j=1,2$,

$$\begin{aligned} &\partial_j f(\nabla f\cdot(\mathbf{u}^{(1)}+\mathbf{u}^{(2)})+\partial_t f)\\ &\quad-\alpha^{(2)}U_j^{(2)} = 0 \text{ in } \Omega\times(0,1)\,. \end{aligned} \tag{29}$$

Thus the optimality conditions for a minimizer, derived by applying the fundamental lemma of calculus of variations, are (28) and (29).

5 Optical flow decomposition in 1D

In order to make transparent the features of our decomposition we study exemplary the one dimensional case. From regularization theory (see e.g. (Scherzer et al, 2009)) we know that the minimizers $(u^{(1)}(\alpha^{(1)},\alpha^{(2)}),\, u^{(2)}(\alpha^{(1)},\alpha^{(2)}))$, for $(\alpha^{(1)},\alpha^{(2)}) \to 0$, are converging to a solution of the optical flow equation which minimizes $\mathcal{R}^{(1)} + \alpha\mathcal{R}^{(2)}$ if $\alpha = \lim_{\alpha^{(1)},\alpha^{(2)}\to 0} \frac{\alpha^{(2)}}{\alpha^{(1)}} > 0$. Such a solution is called $(\mathcal{R}^{(1)}, \alpha\mathcal{R}^{(2)})$ minimizing solution. Note that by the 1D simplification the modules $u^{(i)}$, $i = 1, 2$ are single valued functions.

We calculate the decomposition for the one dimensional optical flow equation (10), for the specific test data (11).The regularized solutions approximate these $(\mathcal{R}^{(1)}, \alpha\mathcal{R}^{(2)})$ minimizing solution, and thus these calculations can be viewed representative for the properties of the regularization method. For these particular data the optical flow equation simplifies to

$$\partial_x \tilde{f}(x) g(t) u(x,t) + \tilde{f}(x)\partial_t g(t) = 0 \,.$$

And therefore

$$u(x,t) = -\frac{\tilde{f}(x)}{\partial_x \tilde{f}(x)} \frac{\partial_t g(t)}{g(t)} = -\frac{\partial_t(\log g)(t)}{\partial_x(\log \tilde{f})(x)} \,. \tag{30}$$

We introduce the anti-derivative of $\partial_t(\log g)$, and assume that it is expandable into a Fourier sin-series:

$$G(t) = \int_0^t \partial_t(\log g)(\tau)\, d\tau = \sum_{n=1}^{\infty} G_n \sin(n\pi t) \,. \tag{31}$$

Moreover, we assume that $\frac{1}{\partial_x(\log \tilde{f})(x)}$ can be expanded in a cos-series:

$$\frac{1}{\partial_x(\log \tilde{f})(x)} = \sum_{m=0}^{\infty} F_m \cos(m\pi x) \,. \tag{32}$$

Then

$$\begin{aligned} -\frac{G(t)}{\partial_x(\log \tilde{f})(x)} &= \int_0^t u(x,\tau)\mathrm{d}\tau \\ &= \int_0^t u^{(1)}(x,\tau)\mathrm{d}\tau + \int_0^t u^{(2)}(x,\tau)\mathrm{d}\tau \\ &=: U^{(1)}(x,t) + U^{(2)}(x,t) \,. \end{aligned} \tag{33}$$

Inserting (33) in the definition of $\mathcal{R}$,

$$\begin{aligned} \mathcal{R}(u^{(1)}, u^{(2)}) := \int_{(0,1)\times(0,1)} & (u_x^{(1)})^2 + (u_t^{(1)})^2 \\ & + \alpha \left(\int_0^t u^{(2)}(x,\tau)\mathrm{d}\tau \right)^2 \mathrm{d}x\mathrm{d}t \,, \end{aligned}$$

we remove the $u^{(2)}$ dependency. In addition, we express the functional $\mathcal{R}$ as a functional of the primitive of $u^{(1)}$ with respect to time (for the sake of simplicity we keep the notation $\mathcal{R}$):

$$\mathcal{R}(U^{(1)}) := \int_{(0,1)\times(0,1)} (U^{(1)}_{xt}(x,t))^2 + (U^{(1)}_{tt}(x,t))^2 + \alpha \left(\frac{G(t)}{\partial_x (\log \tilde{f})(x)} + U^{(1)}(x,t) \right)^2 \mathrm{d}x\mathrm{d}t \,,$$

where we enforce the boundary conditions:

- The first one is due to the choice of $U^{(1)}$ as a time integration from 0 to t of the function $u^{(1)}$:

$$U^{(1)}(x,0) = \int_0^t u^{(1)}(x,\tau)\, d\tau \bigg|_{t=0} = 0 \;.$$

- The second one is an assumption made to simplify the computations:

$$U^{(1)}(x,1) = \int_0^1 u^{(1)}(x,\tau)\, d\tau = 0 \;.$$

  In fact, the assumption seems reasonable because of the choice of G, when the series $\sum_{n=0}^{\infty} G_n$ is absolutely convergent, which implies that $G(1) = 0$. In this case $U^{(1)}(x,1) + U^{(2)}(x,1) = 0$, which is guaranteed by $U^{(1)}(x,1) = U^{(2)}(x,1) = 0$.

By this substitution we reduce the constraint optimization problem to an unconstrained optimization problem for $U^{(1)}$. The optimality condition shows then that $U^{(1)}$ has to satisfy the partial differential equation

$$U^{(1)}_{ttxx} + U^{(1)}_{tttt} + \alpha \left(\frac{G(t)}{\partial_x (\log \tilde{f})(x)} + U^{(1)} \right) = 0 \text{ in } (0,1)\times(0,1)\,,$$

together with the boundary conditions:

$$\begin{aligned} U^{(1)}_{tt} = U^{(1)} &= 0 \text{ on } (0,1)\times\{0,1\} \;, \\ \partial_n U^{(1)}_{tt} &= 0 \text{ on } \{0,1\}\times(0,1) \;. \end{aligned} \tag{34}$$

Now, we substitute

$$W := U^{(1)}_{tt} \,, \tag{35}$$

and we get the following system of equations

$$\begin{aligned} W_{xx} + W_{tt} &= -\alpha \left(\frac{G(t)}{\partial_x (\log \tilde{f})(x)} + U^{(1)} \right) \\ &\quad \text{in } (0,1)\times(0,1)\,, \\ \partial_n W &= 0 \text{ on } \{0,1\}\times(0,1)\,, \\ W &= 0 \text{ on } (0,1)\times\{0,1\} \;, \end{aligned} \tag{36}$$

and

$$\begin{aligned} U^{(1)}_{tt} &= W \text{ in } (0,1)\times(0,1)\,, \\ U^{(1)} &= 0 \text{ on } (0,1)\times\{0,1\} \;. \end{aligned} \tag{37}$$

That is

$$\begin{aligned}U^{(1)}(x,t) = &\int_0^t \int_0^\tau W(x,\hat{\tau})\mathrm{d}\hat{\tau}\mathrm{d}\tau \\ &- t\int_0^1 \int_0^\tau W(x,\hat{\tau})\mathrm{d}\hat{\tau}\mathrm{d}\tau \;.\end{aligned}$$

W can be expanded as follows:

$$W(x,t) = \sum_{m,n=0}^{\infty} W_{mn} \cos(m\pi x)\sin(n\pi t)\,,$$

and we expand $U^{(1)}$ in an analogous manner:

$$U^{(1)}(x,t) = \sum_{m,n=0}^{\infty} U_{mn}^{(1)} \cos(m\pi x)\sin(n\pi t)\;,$$

such that (35) implies that

$$W_{mn} = -n^2\pi^2 U_{mn}^{(1)} \text{ for all } m,n \in \mathbb{N}_0\;. \tag{38}$$

Because of (30) the function $U^{(1)}$ is a product of functions in space and time, respectively, and thus it follows that

$$U^{(1)}(x,t) = \sum_{m=0}^{\infty} U_m^{(1,x)} \cos(m\pi x) \sum_{n=1}^{\infty} U_n^{(1,x)} \sin(n\pi t)\;,$$

or in other words:

$$U_{mn}^{(1)} = U_m^{(1,x)} U_n^{(1,t)}\;.$$

Consequently also

$$W_{mn} = W_m^{(x)} W_n^{(t)}\,,$$

which satisfies, because of (36),

$$\begin{aligned}&W_m^{(x)} W_n^{(t)} (m^2+n^2)\pi^2 \\ &= \alpha\left(U_m^{(1,x)} U_n^{(1,t)} + F_m G_n\right)\;, \\ &\quad\text{for all } m,n \in \mathbb{N}_0\;.\end{aligned} \tag{39}$$

(39) and (38) imply that

$$\begin{aligned}U_m^{(1,x)} U_n^{(1,t)} &= -\frac{\alpha}{\alpha + \pi^4(m^2+n^2)n^2} F_m G_n\,, \\ &\quad\text{for all } m,n \in \mathbb{N}_0\;.\end{aligned} \tag{40}$$

Now, consider a specific test example:

$$g(t) = \exp\left\{\frac{\sin(n_0\pi t)}{n_0\pi}\right\} \text{ with } n_0 \in \mathbb{N}\;.$$

Then, from (30) it follows that

$$u(x,t) = -\frac{\cos(n_0\pi t)}{\partial_x(\log\tilde{f})(x)}\,,$$

and correspondingly we have

$$G(t) = \int_0^t \partial_t (\log g)(\tau)\, d\tau = \frac{\sin(n_0 \pi t)}{n_0 \pi} \ .$$

In this case it follows from (40) that

$$U_m^{(1,x)} = -\frac{\alpha}{\alpha + \pi^4 (m^2 + n_0^2) n_0^2} \frac{G_{n_0}}{U_{n_0}^{(1,t)}} F_m \ .$$

Moreover, from (40) it follows with $m = 0$:

$$\frac{U_{n_0}^{(1,t)}}{G_{n_0}} = -\frac{\alpha}{\alpha + \pi^4 n_0^4} \frac{F_0}{U_0^{(1,x)}} \ .$$

Using the last two equalities, we get

$$U_m^{(1,x)} = \frac{\alpha + \pi^4 n_0^4}{\alpha + \pi^4 (m^2 + n_0^2) n_0^2} \frac{U_0^{(1,x)}}{F_0} F_m \ .$$

The last equality means that the Fourier coefficients of $U^{(1,x)}$ are decreased by a factor $\mathcal{O}\left(\frac{\alpha+\pi^4 n_0^4}{\alpha+\pi^4(m^2+n_0^2)n_0^2}\right)$ relative to F_m.

From this equality we also see that spatial components belonging to Fourier-cos coefficients with large m are more pronounced in the $u^{(2)}$ component. Note that for small m relative to n_0 the factor $\frac{\alpha+\pi^4 n_0^4}{\alpha+\pi^4(m^2+n_0^2)n_0^2} \sim 1$, and thus these components appear almost exclusively in $u^{(1)}$.

These considerations indicate that for assigning a flow component to $\mathbf{u}^{(1)}, \mathbf{u}^{(2)}$, respectively, one has to apply a certain threshold to the single components. This observation is central to perform an appropriate visualization, which is implemented below.

6 Numerics

In this section we discuss the numerical minimization of the energy functional $\mathcal{F}$ defined in (16). Our approach is based on solving the optimality conditions for the minimizer $u_j^{(i)}$, $i, j = 1, 2$ from (28), (29) with a fixed point iteration.

We have stated above that, in general, the optical flow equation can never be well-defined on the whole domain $\Omega \times (0, 1)$. In order to have a consistent approximation of (1), the optical flow equation (3) has to be considered on constrained sets, such as (9). Because we want to apply optical flow computations blindly, without estimating singularities of f and singularities of characteristics first, we apply standard optical flow inversion and evaluate the outcome numerically. The numerical examples actually show that flickering predominantly appears in the $\mathbf{u}^{(2)}$ component, and thus can be used as a guess for the *singularity* sets.

For the purpose of numerical realization of the fixed point iteration we call the iterates of the fixed point iteration $u_j^{(i)}(\mathbf{x}, t; k), U_j^{(2)}(\mathbf{x}, t; k)$, for $k = 1, 2, \ldots, K$, where K denotes the maximal number of iterations. We summarize all iterates of the components of flow functions $u_j^{(i)}$ in a tensor of size $M \times N \times T \times K$. In this section we use the notation as reported in table 1.

$f = f(r,s,t) \in \mathbb{R}^{M\times N\times T}$	Input sequence
$\mathbf{u}^{(i)} = \mathbf{u}^{(i)}(r,s,t;k) \in \mathbb{R}^{M\times N\times T\times K\times 2}$	artificial optical flow module
$\mathbf{u}^{(i)} = \mathbf{u}^{(i)}(r,s,t) = \mathbf{u}^{(i)}(r,s,t;K)$ $\in \mathbb{R}^{M\times N\times T\times 2}$	formal relation between artificial and optical flow module
$u_j^{(i)} = u_j^{(i)}(r,s,t;k) \in \mathbb{R}^{M\times N\times T\times K}$	component of artificial optical flow module
$u_j^{(i)} = u_j^{(i)}(r,s,t) = u_j^{(i)}(r,s,t;K)$ $\in \mathbb{R}^{M\times N\times T}$	formal relation between components of artificial and optical flow module
∂_k^h	Finite difference approximation in direction x_k
∂_t^h	Finite difference approximation in direction t

Table 1: Discrete Notation

For every tensor $H = (H(r,s,t)) \in \mathbb{R}^{M\times N\times T}$ (representing a complete movie) we define the discrete gradient

$$\begin{aligned}\nabla_3^h H(r,s,t) = (\partial_1^h H(r,s,t), \partial_2^h H(r,s,t), \partial_t^h H(r,s,t))^T\,,\\ \text{for } (r,s,t) \in \mathbb{R}^{M\times N\times T}\,,\end{aligned}$$

where

$$\begin{aligned}\partial_1^h H(r,s,t) =& \frac{H(r+1,s,t) - H(r-1,s,t)}{2\Delta_x}\\ & \text{if } 1 < r < M\\ \partial_2^h H(r,s,t) =& \frac{H(r,s+1,t) - H(r,s-1,t)}{2\Delta_y}\\ & \text{if } 1 < s < N\\ \partial_t^h H(r,s,t) =& \frac{H(r,s,t+1) - H(r,s,t)}{\Delta_t}\\ & \text{if } 1 < t < T\end{aligned} \tag{41}$$

where $\Delta_x = \frac{1}{M-1}$, $\Delta_y = \frac{1}{N-1}$ and $\Delta_t = \frac{1}{T-1}$. Moreover, we define the discrete divergence, which is the adjoint of the discrete gradient: Let $(H_1, H_2, H_3)^T(r,s,t)$, then

$$\begin{aligned}\nabla_3^h \cdot (H_1,H_2,H_3)^T(r,s,t) = \partial_1^h H_1(r,s,t) + \partial_2^h H_2(r,s,t)\\ + \partial_t^{h*} H_3(r,s,t)\,,\end{aligned} \tag{42}$$

where

$$\partial_t^{h*} H_3(r,s,t) = \frac{H(r,s,t+1) - H(r,s,t)}{\Delta_t}\,. \tag{43}$$

The implementation used for $\nabla_3^h \cdot (H_1,H_2,H_3)^T(r,s,t)$ is similarly to (Weickert and Schnörr, 2001b). The realization of the fixed point iteration reads as follows:

- $k = 0$: we initialize two flow components $\mathbf{u}^{(1)}(\cdot;0)$, $\mathbf{u}^{(2)}(\cdot;0) \in \mathbb{R}^{M\times N\times K\times 2}$.

– $k \to k+1$: let us denote $\psi'^{(k)} = \psi'(|\nabla_3^h u_1^{(1)}(\cdot;k)|^2 + |\nabla_3^h u_1^{(2)}(\cdot;k)|^2)$, and let Δ_τ be the step size in t direction, then

$$\begin{aligned} &\frac{u_1^{(1)}(\cdot;k+1) - u_1^{(1)}(\cdot;k)}{\Delta_\tau} \\ =&\nabla_3^h \cdot \left(\psi'^{(k)} \nabla_3^h u_1^{(1)}(\cdot;k)\right) \\ &- \frac{\partial_1^h f}{\alpha^{(1)}} \left(\partial_1^h f \left(u_1^{(1)}(\cdot;k+1) + u_1^{(2)}(\cdot;k) \right) \right. \\ &\left. + \partial_2^h f \left(u_2^{(1)}(\cdot;k) + u_2^{(2)}(\cdot;k) \right) + \partial_t^h f \right), \end{aligned} \tag{44}$$

$$\begin{aligned} &\frac{u_2^{(1)}(\cdot;k+1) - u_2^{(1)}(\cdot;k)}{\Delta_\tau} \\ =&\nabla_3^h \cdot (\psi'^{(k)} \nabla_3^h u_2^{(1)}(\cdot;k)) \\ &- \frac{\partial_2^h f}{\alpha^{(1)}} \left(\partial_1^h f \left(u_1^{(1)}(\cdot;k+1) + u_1^{(2)}(\cdot;k) \right) \right. \\ &\left. + \partial_2^h f \left(u_2^{(1)}(\cdot;k+1) + u_2^{(2)}(\cdot;k) \right) + \partial_t^h f \right), \end{aligned} \tag{45}$$

$$\begin{aligned} &\frac{u_1^{(2)}(\cdot;k+1) - u_1^{(2)}(\cdot;k)}{\Delta_\tau} \\ =& - \frac{\partial_1^h f}{\alpha^{(2)}} \left(\partial_1^h f \left(u_1^{(1)}(\cdot;k+1) + u_1^{(2)}(\cdot;k+1) \right) \right. \\ &\left. + \partial_2^h f \left(u_2^{(1)}(\cdot;k+1) + u_2^{(2)}(\cdot;k) \right) + \partial_t^h f \right) \\ &+ U_1^{(2)}(\cdot;k), \end{aligned} \tag{46}$$

and

$$\begin{aligned} &\frac{u_2^{(2)}(\cdot;k+1) - u_2^{(2)}(\cdot;k)}{\Delta_\tau} \\ =& - \frac{\partial_2^h f}{\alpha^{(2)}} \left(\partial_1^h f \left(u_1^{(1)}(\cdot;k+1) + u_1^{(2)}(\cdot;k+1) \right) \right. \\ &\left. + \partial_2^h f \left(u_2^{(1)}(\cdot;k+1) + u_2^{(2)}(\cdot;k+1) \right) + \partial_t^h f \right) \\ &+ U_2^{(2)}(\cdot;k), \end{aligned} \tag{47}$$

where (compare with (25))

$$U_j^{(2)}(r,s,t;k) = -\sum_{\tau=t}^{1} \sum_{\tilde{\tau}=0}^{\tau} u_j^{(2)}(r,s,\tilde{\tau};k), \qquad j = 1,2 .$$

The system (44),(45),(46),(47) can be solved efficiently using the special structure of the matrix equation similarly to (Weickert and Schnörr, 2001a,b).

The iterations are stopped when the Euclidean norm of the relative error

$$\frac{|u_j^{(i)}(\cdot,k) - u_j^{(i)}(\cdot,k+1)|}{|u_j^{(i)}(\cdot,k)|}\,, \qquad j = 1,2$$

drops below the precision tolerance value $tol = 0.01$ for at least one of the component of $\mathbf{u}^{(1)}$ and one of $\mathbf{u}^{(2)}$. The typical number of iterations is below 100, but if we relax the accuracy requirement the process stops much earlier.

7 Reformulation of optical flow computation as a denoising problem

The following outline is taken from (Abhau et al, 2009). The matrix $A_0 := \nabla f(\nabla f)^T$ has rank one, is symmetric and positive semi-definite with non-trivial kernel. The kernel consists of all vector valued functions, which are orthogonal to ∇f. Moreover, let A be an approximation with full rank - see (Bruhn , 2006; Weickert et al, 2006) for details of constructing reasonable approximations.

Defining

$$\hat{\mathbf{f}} = \begin{pmatrix} \hat{\mathbf{f}}_1 \\ \hat{\mathbf{f}}_2 \end{pmatrix} := -\partial_t f \frac{\nabla f}{|\nabla f|}\,, \tag{48}$$

and noting that

$$\begin{aligned} \left(\frac{1}{|\nabla f|}A_0\right)^2 &= \frac{1}{|\nabla f|^2}A_0A_0 \\ &= \frac{1}{|\nabla f|^2}\nabla f\left((\nabla f)^T\nabla f\right)(\nabla f)^T \\ &= \nabla f(\nabla f)^T = A_0\,. \end{aligned}$$

Thus

$$\frac{1}{|\nabla f|^2}A_0^2 = A_0\,,$$

or in other words

$$A_0^{1/2} = \frac{1}{|\nabla f|}A_0\,.$$

Thus it follows that

$$\begin{aligned} &\left\| A_0^{1/2}\cdot\mathbf{u} - \hat{\mathbf{f}}\right\|^2_{L^2(\Omega;\mathbb{R}^2)} \\ =& \int_\Omega [(A_0^{1/2}\cdot\mathbf{u})_1 - \hat{\mathbf{f}}_1]^2 + [(A_0^{1/2}\cdot\mathbf{u})_2 - \hat{\mathbf{f}}_2]^2 \mathrm{d}\mathbf{x} \\ =& \int_\Omega \left[\frac{(\partial_1 f)^2u_1 + \partial_1 f\partial_2 f u_2}{|\nabla f|} + \frac{\partial_1 f\partial_t f}{|\nabla f|}\right]^2 + \\ &\qquad + \left[\frac{\partial_1 f\partial_2 f u_1 + (\partial_2 f)^2u_2}{|\nabla f|} + \frac{\partial_2 f\partial_t f}{|\nabla f|}\right]^2\mathrm{d}\mathbf{x} \\ =& \int_\Omega \frac{(\partial_1 f)^2 + (\partial_2 f)^2}{|\nabla f|^2}(\partial_1 f u_1 + \partial_2 f u_2 + \partial_t f)^2\mathrm{d}\mathbf{x} \\ =& \|\nabla f\cdot\mathbf{u} + \partial_t f\|^2_{L^2(\Omega)}\,, \end{aligned} \tag{49}$$

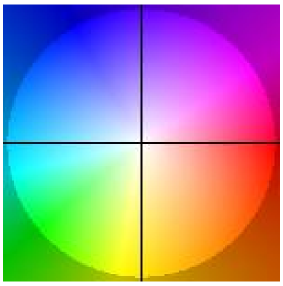

Fig. 5: Color wheel

Then, by using the notation

$$\tilde{\mathbf{f}} = A^{-\frac{1}{2}}\hat{\mathbf{f}}\,, \tag{50}$$

we find that, taking into account that A is symmetric and that $A_0 \approx A$, that

$$\begin{aligned}
&\|\nabla f \cdot \mathbf{u} + \partial_t f\|^2_{L^2(\Omega)} \\
&= \left\| A_0^{1/2} \cdot \mathbf{u} - A^{1/2} A^{-1/2} \hat{\mathbf{f}} \right\|^2_{L^2(\Omega;\mathbb{R}^2)} \\
&\approx \int_\Omega (\mathbf{u} - A^{-1/2}\hat{\mathbf{f}})^T A^{1/2T} A^{1/2} (\mathbf{u} - A^{-1/2}\hat{\mathbf{f}})\, d\mathbf{x} \\
&=: \left\| \mathbf{u} - \tilde{\mathbf{f}} \right\|^2_A \,.
\end{aligned} \tag{51}$$

This relation shows that the optical flow least squares functional $\mathcal{S}$ defined in (4) can be approximated, and in fact replaced, by the squared norm of the weighted L^2-space induced by A. The bottom line of these calculations are that optical flow computations can be viewed as a least squares denoising problem. This analogy will be used to evaluate the numerical experiments below. It shows, in particular, how the algorithms processes data, with significant perturbations, such as flickering.

8 Experiments

In this section we present numerical experiments to demonstrate the potential of the proposed optical flow decomposition model. In the first two experiments we use for visualization of the computed flow fields the standard flow color coding (Baker et al, 2011). The flow vectors are represented in color space via the color wheel illustrated in Figure 5. For the third and fourth experiments we use a black and white visualization technique. Moreover, a black color is assigned to pixels where no flow is present and a gray-shade color elsewhere. The shade is chosen proportional to the flow magnitude.

In order to compare frequencies of the sequences used for testing, it is necessary to have the same scaling over space and time. For this reason, all the intensity values, the domain Ω, and the time are scaled in the range $[0, 1]$. The used parameters are reported for each experiment except for $\Delta_x, \Delta_y, \Delta_t$ defined as in Section 6. In this work we consider the following four dynamic image sequences:

Fig. 6: Top: Optical flow decomposition $\mathbf{u} = \mathbf{u}^{(1)} + \mathbf{u}^{(2)}$ between the 15th and the 16th frame with $\alpha^{(2)} >> \alpha^{(1)}$ parameter setting composed of $\alpha^{(1)} = 10^{-5}$, $\alpha^{(2)} = 1000$, $\Delta_\tau = 10^{-4}$, precision tolerance $tol = 0.05$. The optical flow computation shows that the whole ball is rotating, while standard optical flow methods calculate the local optical flow representing a local movement.
Bottom: the optical flow calculated with Weickert-Schnörr between the 15th and the 16th frame $\alpha^{(1)} = 10^{-5}$, $\Delta_\tau = 10^{-4}$, precision tolerance $tol = 0.05$. One sees in this frame only the local movement of the stains on the sphere.

- The first tests are performed with the video sequence from (McCane et al, 2001) (available at http://of-eval.sourceforge.net/) which consists of forty-six frames showing a rotating sphere with some overlaid patterns. We performed two experiments:
  - We study the behaviour of the optical flow model when $\alpha^{(1)} >> \alpha^{(2)}$ and $\alpha^{(2)} >> \alpha^{(1)}$. In this case the complete flow $\mathbf{u}^{(1)} + \mathbf{u}^{(2)}$ of the decomposition method recovers a global uniform movement. Figure 6 shows the reconstruction for $\alpha^{(2)} >> \alpha^{(1)}$.

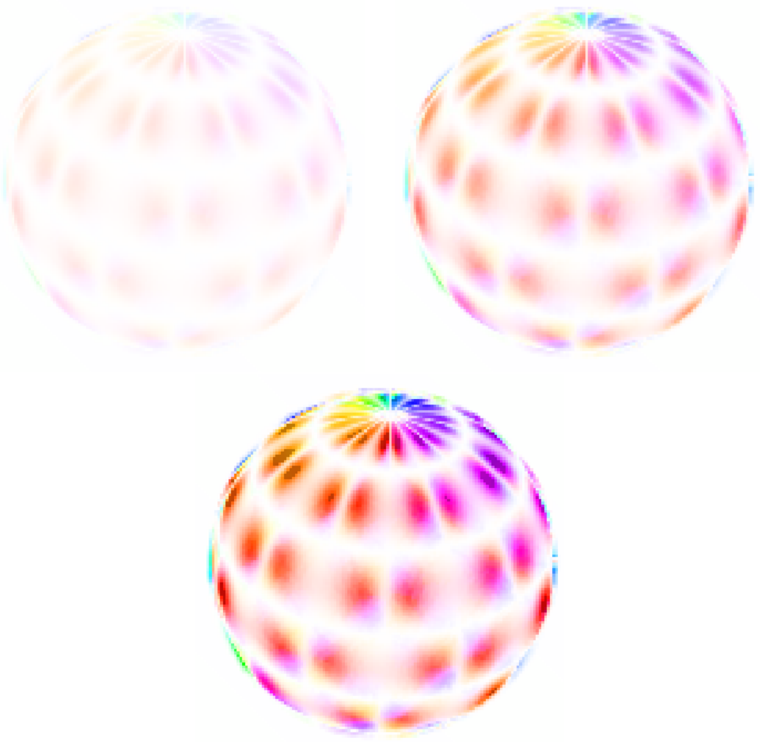

Fig. 7: $\mathbf{u}^{(2)}$ at different frequencies of rotations: original frequency, 4 and $8\times$ faster. $\alpha^{(1)} = 1$, $\alpha^{(2)} = \frac{1}{4}$, $\Delta_\tau = 10^{-4}$ and precision tolerance $tol = 0.05$. The intensity of $\mathbf{u}^{(2)}$ increases when the frequency of rotation is increased. At the same time $\mathbf{u}^{(1)}$ stays always very small.

- The analytical results from Section 5 in 1D show that the intensity of the $\mathbf{u}^{(2)}$ component increases monotonically with repetitiveness over time. We verify this hypothesis numerically in higher dimensions. We simulate in particular two, four and eight times the original motion frequency. In order to do so, we duplicate the sequence periodically, however consider it to be in the same time interval $(0, 1)$. The flow visualized in Figure 7 is the one between the 16th and the 17th frame of every sequence. Since the sampling of the sequences is different, we decide to choose a precise configuration of the sphere in order to ensure the comparability of the results. The optical flow shown in Figure 7 is the one relative to the above described configuration for different sampling of the original sequence. We study the behaviour of the sphere at different motion frequencies with the same parameter setting $\alpha^{(1)} = 1$, $\alpha^{(2)} = \frac{1}{4}$, $\Delta_\tau = 10^{-4}$, precision tolerance $tol = 0.05$. This confirms the results of the $1D$ example that high frequencies are dominantly visible in $\mathbf{u}^{(2)}$ (cf. Figures 7). Because the movement is periodic, $\mathbf{u}^{(2)}$ is the dominant part, and $\mathbf{u}^{(1)}$ is always very small, such that it disappears after thresholding.

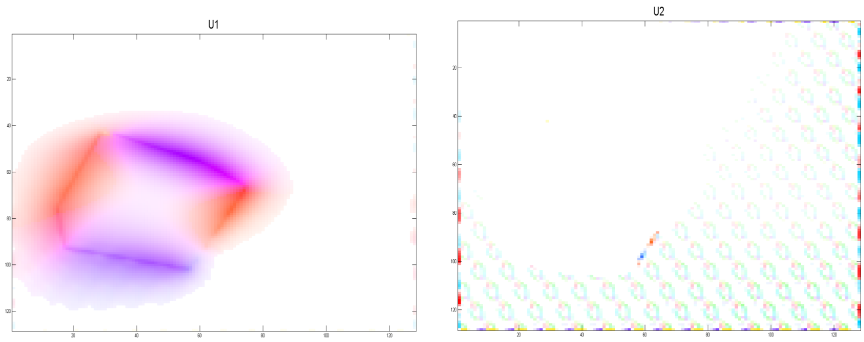

Fig. 8: The dynamic sequence consists of the smooth (translation like) motion of a cube and an oscillating background. The oscillation has a periodicity of four frames and takes place along the diagonal direction from the bottom left to the top right, moving at a rate of 5% of the frame size in each frame. The proposed model decomposes the motion, obtaining the global movement of the cube in $\mathbf{u}^{(1)}$ (top) and the background movement solely in $\mathbf{u}^{(2)}$ (bottom).

– The second experiment concerns the decomposition of the motion in a dynamic image sequence showing a projection of a cube moving over an oscillating background. The movie consists of sixty frames and can be viewed on the web-page http://www.csc.univie.ac.at/index.php?page=visualattention. The background is oscillating in diagonal direction, from the bottom left to the top right, with a periodicity of four frames. In each frame the oscillation has a rate of 5% of the frame size. The flow visualized in 8 is the one between the twentieth and the twenty-first frame of the sequence. Applying the proposed method with a parameter setting $\alpha^{(1)} = 10^3$, $\alpha^{(2)} = 10^3$, $\varDelta_\tau = 10^{-5}$, and precision tolerance $tol = 0.001$, we notice that the background movement appears almost solely in $\mathbf{u}^{(2)}$ and the global movement of the cube appears in $\mathbf{u}^{(1)}$. In Figure 8 we represent only flow vectors with magnitude larger than 0.05 and omit in $\mathbf{u}^{(2)}$ the part in common with $\mathbf{u}^{(1)}$ for better visibility. This is exactly the behaviour expected from the analytical example 5, showing the ability of the model to divide patterns relative to frequencies.
– The third experiment is relative to the decomposition of the flow in a dynamic image sequence showing a real scene. The original movie consists of thirty-two frames and can be viewed together with the decomposition result on the web-page
http://www.csc.univie.ac.at/index.php?page=visualattention. The movement present in the movie can be decomposed in a smooth and an oscillating part. The smooth part represents the movement of a Ferris wheel and people walking. The oscillating one is composed of lights blinking and the reflection of the wheel on the glass. The flow visualized in Figure 9 is the one between the fourth and the fifth frame of the sequence with a parameter setting $\alpha^{(1)} = 1$, $\alpha^{(2)} = \frac{1}{4}$, $\varDelta_\tau = 10^{-4}$, and precision tolerance $tol = 0.05$. In order to improve the visibility we represent only flow vectors with magnitude larger than 0.18 and omit in $\mathbf{u}^{(2)}$ the part in common with $\mathbf{u}^{(1)}$. We notice that the smooth movement appears in $\mathbf{u}^{(1)}$, while the oscillating movement solely appears in

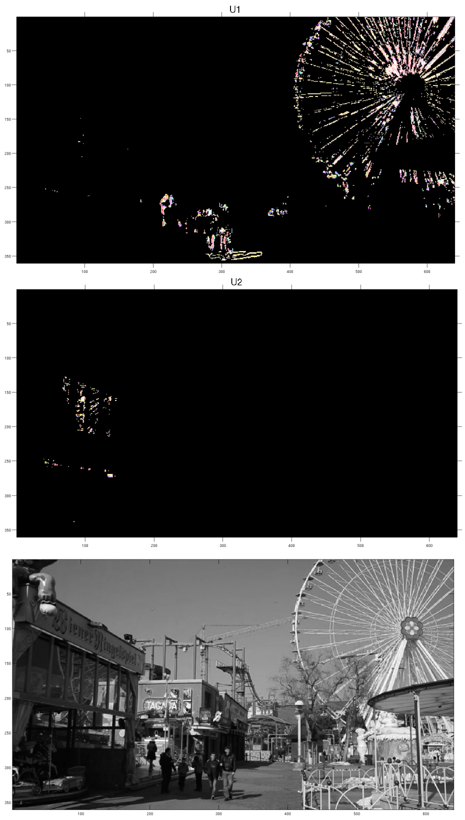

Fig. 9: The movement in the dynamic sequence is composed of a smooth (oscillating) motion $\mathbf{u}^{(1)}$ of a Ferris wheel and people walking in the foreground (top). Moreover, the second component $\mathbf{u}^{(2)}$ consists of blinking lights and the reflections of the wheel on glass (middle). The third image (bottom) is a reference frame.

$\mathbf{u}^{(2)}$. On the one hand, it is worth noting that $\mathbf{u}^{(1)}$ is not able to capture the information about the blinking lights and the reflection of the wheel. This is due to the fact that the movement is not smooth and $\mathcal{R}^{(1)}$ ignores therefore this information. On the other hand, $\mathcal{R}^{(2)}$ is designed for detecting oscillating pattern, so $\mathbf{u}^{(2)}$ captures the movements ignored by $\mathbf{u}^{(1)}$. The evidence presented above suggests that the proposed model allows the use of the data in a dynamic sequence in a better way, thanks to the detection of oscillating patterns. Let us concentrate on neighborhood of the blinking regions. Outside the region the flow should be the 0 and the deformation is the identity over the whole time interval. The blinking region determine characteristics of the deformation which are interrupted and with appropriate time scaling they appear like local soft-flickering. Therefore we expect to see them in the $\mathbf{u}^{(2)}$ component.

– The fourth example is a flickering experiment. In a standard flickering experiment, the difference in human attention is investigated by inclusion of blank images in a repetitive image sequence. Although, in general, these blank images are not deliberately recognized, they change the awareness of the test persons. The proposed optical flow decomposition, as we show in this section, is able to detect moving regions, which humans can also recognize. At the same time, standard optical flow models fail. Motivated by the work of J. K. O'Regan (O'Regan, 2007), we have tested the decomposition model on flicker data from `http://nivea.psycho.univ-paris5.fr`. In practice, as reported by J. K. O'Regan: "*Change blindness is a phenomenon in which a very large change in a picture will not be seen by a viewer, if the change is accompanied by a visual disturbance that prevents attention from going to the change location*". In the sequence used in our test, each frame containing the visual information is alternated with a blank frame, as visual disturbance, so that the user experiences the *change blindness* effect.

Flickering does not seem to be a prime application for **quantitative optical flow computations. We have shown in (Abhau et al, 2009) that quasi-static optical flow computations can be viewed as a high-dimensional denoising problem, with a least-squares fit-to-data term, which depends on a metric induced by the image data. The same formulation can be generalized to dynamic data and reads as in Section 7. In view of this, the Weickert-Schnörr algorithm (Weickert and Schnörr, 2001b) behaves like a diffusion filter, which smooths rough details of the flow. In a simplified setting of a time series at a single point, it behaves like cubic spline fitting of time (see (Hanke et al, 2001)). The proposed optical flow algorithm, as well as the Weickert-Schnörr algorithm therefore are capable of recovery an approximative flow field. The goal of the following example is to show that the computated flow can provide qualitatively correct information.**

Below we make several different flickering experiments:

- For this experiment we scale all input frames (that are two in this case) to a range between $[-1/2, 1/2]$ such that the mean intensity is zero.
  From these images we generate a sequence of four frames, consisting of Frame 1, a blank image, Frame 2 and again an identical blank image. This sequence is then aligned periodically to a movie. We call it the 1111 movie. We emphasize that we interpret the movie as a linear interpolation between the frames.
  The first numerical experiments attempt to evaluate the effect of the *intensity* of the inserted blank frame on the optical flow components $\mathbf{u}^{(1)}$ and $\mathbf{u}^{(2)}$.
  If Frame 1 and 3 are identical, the flow is also periodic with a period $\mathbf{u}(\cdot, t_1)$, $\mathbf{u}(\cdot, t_2)$, $-\mathbf{u}(\cdot, t_1) = \mathbf{u}(\cdot, t_3)$, $-\mathbf{u}(\cdot, t_2) = \mathbf{u}(\cdot, t_4)$, where t_i are the times associated with each frame. For such a flow, the penalization functional for $\mathbf{u}^{(2)}$ is vanishing. This, however, is not the case if Frame 1 and Frame 3 are not identical.
  The regularization functional $\mathcal{R}_2$ does not penalize periodic patterns. However, for the flickering, the proposed difference approximations $\Delta_t f$ of ∂_f result in high residuals of the optical flow equation. The error can be minimized if we take a blank sheet with mean values of the image, which is flickered. The results are displayed for different intensity sheets in Figure 10. However, from Example 2 we can expect to see a singularity for every

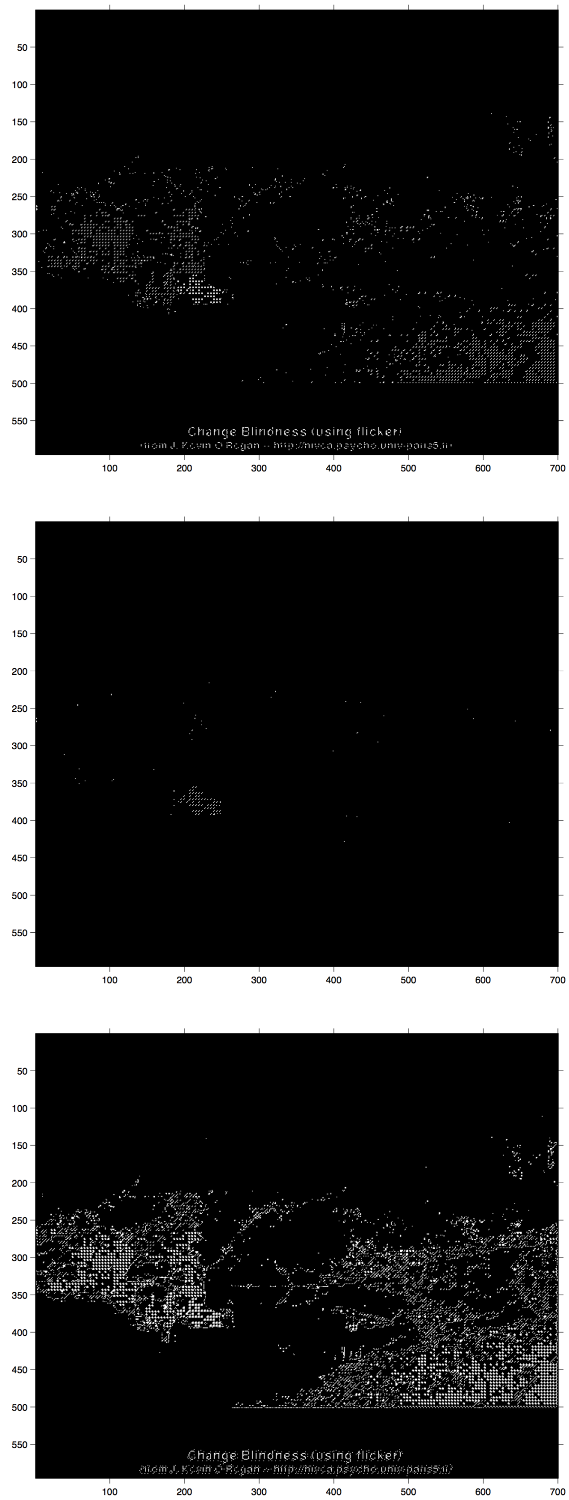

Fig. 10: $\mathbf{u}^{(2)}$ component of the flow for the seventh frame of the 1111 sequence using a white (top), a gray (middle) and a black frame (bottom), respectively. We visualize the flow field, which exceeds a threshold of 0.23 for all the experiments.

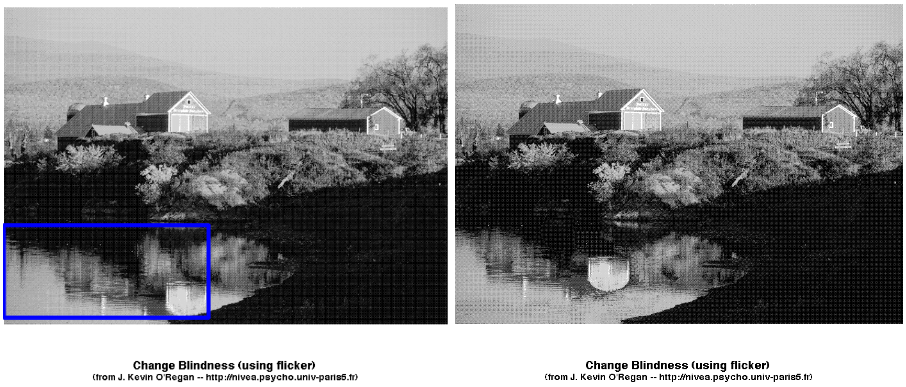

Fig. 11: The two frames of the flickering sequence containing information. In the top image a blue box is superimposed. It indicates the area of special interest that will be analyzed in Figure 12.

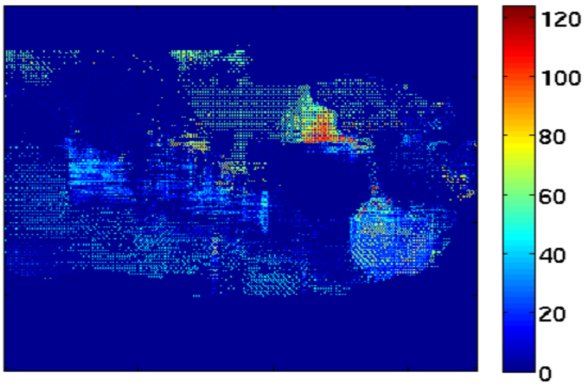

Fig. 12: Difference between the two frames before and after the inclusion of a blank frame. On the original image these are the pixels with row index from 300 to 550 and column index from 1 to 350.

blank frame. This appears for the white and black separating sheets, but not for the gray, mean value, sheet, where there becomes visible the actual difference between the two input frames (cf. Table 2). This observation is interesting from an analytical point of view because the theoretical results predict that in the limiting case the flow should be just the identity.

– We consider now hard flickering. We simulate this by a periodic sequence consisting of periods of $3, 5, 8\times$ of Input Frame 1, a blank frame, $3, 5, 8\times$ of Input Frames 2, respectively.We call these sequences $(3, 5, 8)1(3, 5, 8)$ sequences. Theoretically, in the continuous formulation, for hard flickering, the Weickert-Schnörr algorithm and our algorithm, respectively, should result in $\mathbf{u} \equiv \mathbf{u}_1 \equiv 0$ (cf. Example 1). We would like to understand whether this trend is observable numerically, and in fact this is reflected in Table 3.

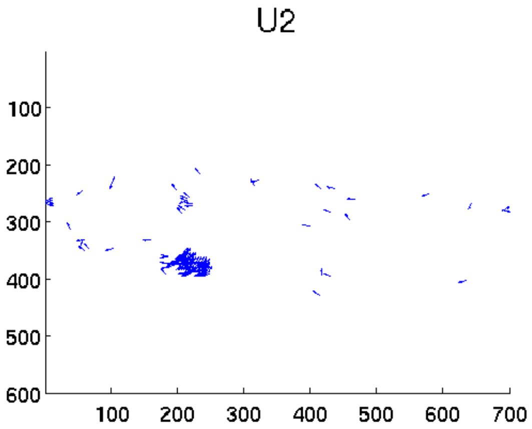

Fig. 13: Flow field $\mathbf{u}^{(2)}$ relative to the 1111 flickering experiment using a quiver visualization. The accumulation of the arrows are on the position of the highest intensity of difference image in Figure 12. It is actually not the mirrors of the house in the lake, because, in black and white, the house gets completely resolved in the lake. Note that the whole region of the mirror is shifted in the lake, and the strongest intensity changes are visualized.

– We also test and compare Horn-Schunck, Weickert-Schnörr and the proposed algorithm. In Horn-Schunck we use the parameter setting $\alpha = 10$ and 200 iterations. In Figure 14 we visualize the flow field, between the blank frame and the slightly changed frame, which exceeds a threshold of 3.9, leading to an obscure result. The Weickert-Schnörr algorithm is tested

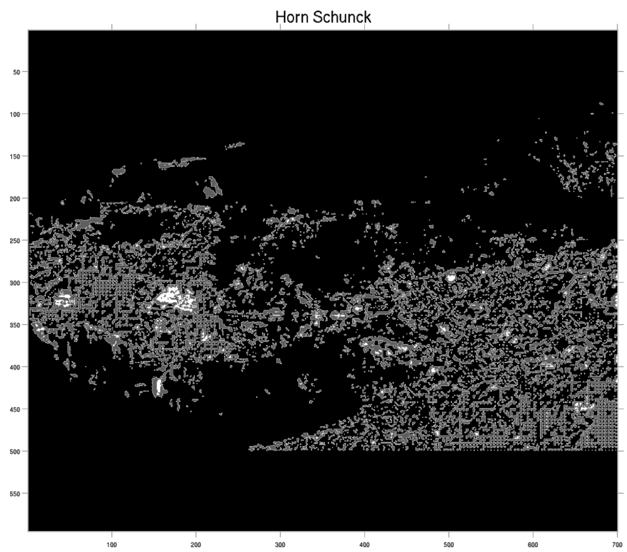

Fig. 14: Result with Horn-Schunck

Frame	Max $u^{(1)}$	Max $u^{(2)}$	Residual
1111 Sequence			
White disturbing frame			
1	0.0799	0.2976	7.6957*10^3
2	0.0036	0.0138	9.3658*10^3
3	0.0805	0.3004	7.6127*10^3
4	0.0037	0.0140	9.4129*10^3
5	0.0797	0.2976	7.6963*10^3
6	0.0036	0.0138	9.3658*10^3
7	0.0805	0.3	7.6140*10^3
Gray disturbing frame			
1	0.0698	0.2542	7.8762*10^3
2	0.0465	0.1682	9.1070*10^3
3	0.0703	0.2566	7.7908*10^3
4	0.0472	0.1707	9.1631*10^3
5	0.0697	0.2541	7.8766*10^3
6	0.0465	0.1682	9.1070*10^3
7	0.0704	0.2563	7.7916*10^3
Black disturbing frame			
1	0.0910	0.3460	7.3570*10^3
2	1.5336*10^-4	0.0022	9.1808*10^3
3	0.0916	0.3494	7.2643*10^3
4	3.0519*10^-4	0.0021	9.2388*10^3
5	0.0908	0.3460	7.3578*10^3
6	4.5800*10^-4	0.0016	9.1808*10^3
7	0.0917	0.3486	7.2660*10^3

Table 2: Comparison for disturbing frames of different intensity in the flicker experiment. In our experiment, the second, forth, sixth frame is blank, such that the gradient vanishes. In this case the optical flow residual is just $\frac{\|f(t_{i+1})-f(t_i)\|}{\Delta_t}$, for $i = 2, 4, 6$, and therefore is identical for $i = 2, 6$ because the same frames are used for evaluation of the residual. In table are reported the maximum values in magnitude for the flow fields $\mathbf{u}^{(1)}$ $\mathbf{u}^{(2)}$ and the corresponding residual value

with the parameter setting $\alpha^{(1)} = 10$, $\Delta_\tau = 10^{-4}$ and precision tolerance $tol = 0.05$. The results obtained by applying Weickert-Schnörr and $\mathbf{u}^{(1)}$ are not visualized, since these components are rather small in magnitude. This behaviour is coherent with the motivation of the Weickert-Schnörr method to produce an optical flow that is less sensitive to variations over space and time. In this flickering example all the objects are varying over space and time, and the average is the zero flow.
For the proposed model we set $\alpha^{(1)} = 1$, $\alpha^{(2)} = \frac{1}{4}$, $\Delta_\tau = 10^{-4}$, precision tolerance $tol = 0.05$, and for visualization we omit all vectors with magnitude lower than 0.23 (see Figure 10(middle)). Additionally, we show in Figure 8 one of the frame of the 1111 sequence with superimposed a blue box. The area highlighted is the one in which we have a change of intensity(cf. Figure 12). Finally we show in Figure 13 the flow field calculated using a quiver plot. We emphasize that $\mathbf{u}^{(1)}$ component is not able to notice the movement, instead $\mathbf{u}^{(2)}$ detects the change.

We remark, that the correct model of the optical flow equation for data including flickering would require to detect the flicker first and then to solve constrained optimization problems within the time frames. If we solve the optical flow equation

Frame	Max $u^{(1)}$	Max $u^{(2)}$	Residual
313 Sequence			
1	1.2906*10^-4	7.2556*10^-4	0
2	8.5145*10^-5	7.2556*10^-4	0
3	0.1115	0.4257	9.9360*10^3
4	0.0735	0.2804	1.2390*10^4
5	1.5736*10^-4	6.0860*10^-4	0
6	4.3081*10^-5	3.3210*10^-4	0
7	2.4397*10^-8	1.6296*10^-8	0
515 Sequence			
1	1.6484*10^-4	9.0007*10^-4	0
2	1.6436*10^-4	9.0007*10^-4	0
3	1.6435*10^-4	9.0007*10^-4	0
4	1.6435*10^-4	8.9067*10^-4	0
5	0.0737	0.2842	3.4946*10^3
6	0.0488	0.1867	4.4600*10^3
7	1.2419*10^-4	9.4929*10^-4	0
8	9.8785*10^-5	7.5451*10^-4	0
9	6.9547*10^-5	5.3135*10^-4	0
10	3.6616*10^-5	2.7981*10^-4	0
11	1.1833*10^-8	7.7489*10^-9	0
818 Sequence			
1	1.9430*10^-4	0.0011	0
2	1.9557*10^-4	0.0011	0
3	1.9559*10^-4	0.0011	0
4	1.9559*10^-4	0.0011	0
5	1.9559*10^-4	0.0011	0
6	1.9555*10^-4	0.0011	0
7	1.8093*10^-4	0.0011	0
8	0.0492	0.1923	1.347*10^3
9	0.0325	0.1259	1.7421*10^3
10	1.6484*10^-4	0.0013	0
11	1.4696*10^-4	0.0011	0
12	1.2710*10^-4	9.8107*10^-4	0
13	1.0539*10^-4	8.1402*10^-4	0
14	8.1821*10^-5	8.8379*10^-4	0
15	5.6395*10^-5	4.3603*10^-4	0
16	3.5540*10^-5	2.7423*10^-4	0
17	5.6939*10^-9	3.7172*10^-9	0

Table 3: Table of comparison for sequences composed of three, five or eight times Frame 1, a gray disturbing frame and three, five or eight times Frame 2.

blindly, then the dominant part of the flow at the blank images is $\mathbf{u}^{(2)}$. As predicted in Section 5 the flow is never separated completely between $\mathbf{u}^{(1)}$ and $\mathbf{u}^{(2)}$, but the dominant part assigns the flow to be the result of a singularity of the image or a singularity of the characteristics. Our numerical experiments show however that it suffices to solve the optical flow equation and detect the flicker by the second flow component. This is what is called relaxation. We have also remarked above that the optical flow (in our case the $\mathbf{u}^{(1)}$- component) is a smooth field and $\mathbf{u}^{(1)}$ and $\mathbf{u}^{(2)}$ only give a tendency. The numerical results for flickering with different arrangement of frames can be viewed to show the effect of course to fine discretization in time.

8.1 Additional Information

In the following, we show the capacity of our model to extract more and different information compared to standard optical flow algorithms. The current literature focuses on average angular and endpoint error(Baker et al, 2011) in order to compare optical flow algorithms. Our proposed model extracts information relative to oscillating patterns, that is usually neglected by standard algorithms. Therefore the focus of our model differs from standard literature.
Such difference can be shown through a quantitative comparison of models. For this purpose, we use well-known test sequences from the Middlebury database `http://vision.middlebury.edu/flow/`, and evaluate the residual of the *optical flow constraint*. We compare the residual of our method with the one of the Horn-Schunck method (Horn and Schunck, 1981), with the following parameter settings:

- We emphasize that the Horn-Schunck method does not use time information, and therefore we calculate for every pair of successive frames and stack the series of flow images into a movie. For calculating the flow for one pair we use the regularization parameter $\alpha = 400$ and 50 iterations for every pair of frames.
- For the proposed method $\alpha^{(1)} = 400$, $\alpha^{(2)} = 10$, $\Delta_\tau = 10^{-4}$ and tolerance value $tol = 0.03$. In this case the whole image sequence is used at once.

The dimension of the parameters $\alpha^{(1)}, \alpha^{(2)}$ is chosen larger than 1 in order to avoid over-fits to the data. For every pair of successive images f_1 and f_2 we visualize the squared residual

$$\int_\Omega \left(\nabla f_1 \cdot \mathbf{u} + \frac{f_2 - f_1}{\Delta_t} \right)^2 \mathrm{d}\mathbf{x}\,,$$

both for Horn-Schunck and the proposed method. Note that for the comparison we omit space dependency of the movie. We notice from Figure 15 that the squared residual is larger in every frame for Horn-Schunck than for our decomposition model, meaning that the proposed method is capable to extract more flow information.

In order to understand how much information our method is capable to extract from an entire dynamic sequence, we also calculate the residual squared over space and time: $\mathcal{E}(\mathbf{u}^{(1)}, \mathbf{u}^{(2)})$ and compare it with the squared residual over space and time of the Weickert-Schnörr method (Weickert and Schnörr, 2001b,a). We use the parameter settings $\alpha^{(1)} = 100$ ($\alpha = \alpha^{(1)}$ in Weickert-Schnörr) and $\alpha^{(2)} = \frac{1}{4}$, $\Delta_\tau = 10^{-4}$ and tolerance $tol = 0.01$, in order to have a good comparison of the two methods. Again the residual is smaller for the proposed method as shown in table 4.

9 Conclusion

We present a new optical flow model for decomposing the flow in spatial and temporal components of different scales. A main ingredient of our work is a new formulation of the optical flow equation, which is assumed to hold on connected domains of characteristics of the nonlinear equation. In the future it is essential to get a better understanding of the optical flow equation in case of singularities of the image data and singular points of the characteristics of the nonlinear equation.

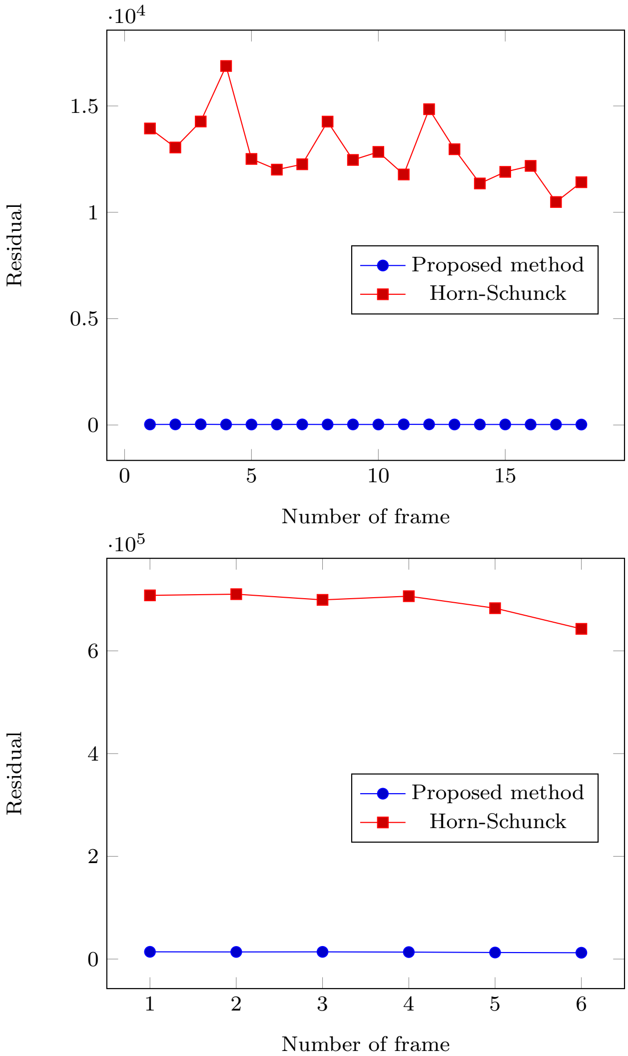

Fig. 15: Residuals for Hamburg taxi (up) and Minicooper sequence (down) from Middlebury database. Residuals for Horn-Schunck are plotted in red, the proposed method is plotted in blue.

Acknowledgment

This work is carried out within the project *"Modeling Visual Attention as a Key Factor in Visual Recognition and Quality of Experience"* funded by the Wiener Wissenschafts und Technologie Fonds - WWTF. OS is also supported by the Austrian Science Fund - FWF, Project S11704 with the national research network, NFN, Geometry and Simulation. The authors would like to thank U. Ansorge, C. Valuch, S. Buchinger, C. Kirisits, P. Elbau, L. Lang, G. Dong, T, Widlak for

	Weickert-Schnörr	Proposed model
Hamburg Taxi	1374.9	1021
RubberWhale	4459.7	3046.8
Hydrangea	8533.3	7647.2
DogDance	9995.4	8217.6
Walking	8077.5	5944.3

Table 4: Comparison of squared residuals over space and time $\mathcal{E}$ between Weickert-Schnörr and the proposed method.

interesting discussions on optical flow and Jose A. Iglesias for discussions and the creation of the cube sequence.

References

Abhau J, Belhachmi Z, Scherzer O (2009) On a decomposition model for optical flow. In: Energy Minimization Methods in Computer Vision and Pattern Recognition, Lecture Notes in Computer Science, vol 5681, Springer-Verlag, Berlin, Heidelberg, pp 126–139, DOI 10.1007/978-3-642-03641-5_10, URL http://dx.doi.org/10.1007/978-3-642-03641-5_10

Andreev R, Scherzer O and Zulehner W (2015) Simultaneous optical flow and source estimation: space-time discretization and preconditioning. RICAM-Report No. 2014-23 URL https://www.ricam.oeaw.ac.at/publications/reports/14/rep14-23.pdf

Aubert G, Aujol JF (2005) Modeling very oscillating signals. Application to image processing. Appl Math Optim 51(2):163–182

Aujol JF, Chambolle A (2005) Dual norms and image decomposition models. Int J Comput Vision 63(1):85–104

Aujol JF, Kang S (2006) Color image decomposition and restoration. J Vis Commun Image Represent 17(4):916–928, DOI 10.1016/j.jvcir.2005.02.001, URL http://www.sciencedirect.com/science/article/B6WMK-4FTWJGT-1/2/ffd97bf7a31e0b9cfdc8af0895369e84

Aujol JF, Aubert G, Blanc-Féraud L, Chambolle A (2005) Image decomposition into a bounded variation component and an oscillating component. J Math Imaging Vision 22(1):71–88

Aujol JF, Gilboa G, Chan T, Osher S (2006) Structure-texture image decomposition—modeling, algorithms, and parameter selection. Int J Comput Vision 67(1):111–136

Baker S, Scharstein D, Lewis JP, Roth S, Black MJ, Szeliski R (2011) A database and evaluation methodology for optical flow. Int J Comput Vision 92(1):1–31, DOI 10.1007/s11263-010-0390-2, URL http://www.springerlink.com/index/10.1007/s11263-010-0390-2

Bauer M, Bruveris M,Michor W.P. (2014) Overview of the geometries of shape spaces and diffeomorphism groups. J Math Imaging Vision 50(1-2):60–97, DOI 10.1007/s10851-013-0490-z, URL http://dx.doi.org/10.1007/s10851-013-0490-z

Berkels B, Effland A and Rumpf M (2015) Time discrete geodesic paths in the space of images. ArXiv URL http://arxiv.org/abs/1503.02001

Borzi A, Ito K, and Kunisch K (2002) Optimal control formulation for determining optical flow. SIAM J Sci Comput 24(3):818–847

Bruhn A (2006) Variational optic flow computation: Accurate modeling and efficient numerics. PhD thesis, Saarland University, Germany

Duval V, Aujol JF, Vese L (2010) Mathematical modeling of textures: Application to color image decomposition with a projected gradient algorithm. J Math Imaging Vision 37:232–248

Hanke M, Scherzer O (2001) Inverse problems light: numerical differentiation. Amer. Math. Monthly 108(6):512–521 DOI 10.2307/2695705, URL http://dx.doi.org/10.2307/2695705

Horn BKP, Schunck BG (1981) Determining optical flow. Artificial Intelligence 17:185–203

Jain A, Younes L, (2013) A kernel class allowing for fast computations in shape spaces induced by diffeomorphisms. J Comput and Applied Math 245:162–181 DOI 10.1016/j.cam.2012.10.019, URL http://dx.doi.org/10.1016/j.cam.2012.10.019

Kohlberger T, Memin E, Schnörr C (2003) Variational dense motion estimation using the helmholtz decomposition. In: Griffin LD, Lillholm M (eds) Scale Space Methods in Computer Vision, Lecture Notes in Computer Science, vol 2695, Springer, Berlin, pp 432–448, DOI 10.1007/3-540-44935-3_30, URL http://dx.doi.org/10.1007/3-540-44935-3_30

McCane B, Novins K, Crannitch D, Galvin B (2001) On benchmarking optical flow. Comput Vision Image Understanding 84:126–143

Meyer Y (2001) Oscillating patterns in image processing and nonlinear evolution equations, University Lecture Series, vol 22. American Mathematical Society, Providence, RI, the fifteenth Dean Jacqueline B. Lewis memorial lectures

Miller M I, Younes L (2001) Group actions, homeomorphisms, and matching: A general framework Int J Comput Vision 41(1/2):61–84,

O'Regan JK (2007) Change blindness. E Cognitive science

Scherzer O, Grasmair M, Grossauer H, Haltmeier M, Lenzen F (2009) Variational methods in imaging, Applied Mathematical Sciences, vol 167. Springer, New York, DOI 10.1007/978-0-387-69277-7, URL http://dx.doi.org/10.1007/978-0-387-69277-7

Sharmin N, Brad R (2012) Optimal Filter Estimation for Lucas-Kanade Optical Flow. Sensors 12(9):12694–12709, DOI 10.3390/s120912694, URL http://www.mdpi.com/1424-8220/12/9/12694

Vese L, Osher S (2003) Modeling textures with total variation minimization and oscillating patterns in image processing. J Sci Comput 19(1–3):553–572, special issue in honor of the sixtieth birthday of Stanley Osher

Vese L, Osher S (2004) Image denoising and decomposition with total variation minimization and oscillatory functions. J Math Imaging Vision 20:7–18

Wang CM, Fan KC, Wang CT (2008) Estimating Optical Flow by Integrating Multi-Frame Information. Journal of Information Science and Engineering 24:1719–1731

Weickert J, Bruhn A, Brox T, Papenberg N (2006) A Survey on Variational Optic Flow Methods for Small Displacements. Mathematical Models for Registration and Applications to Medical Imaging, Springer Berlin Heidelberg 10:103–136 URL http://dx.doi.org/10.1007/978-3-540-34767-5_5

Weickert J, Schnörr C (2001a) A theoretical framework for convex regularizers in PDE-based computation of image motion. Int J Comput Vision 45(3):245–264

Weickert J, Schnörr C (2001b) Variational optic flow computation with a spatio-temporal smoothness constraint. J Math Imaging Vision 14:245–255

Yuan J, Schörr C, Steidl G (2007) Simultaneous higher-order optical flow estimation and decomposition. SIAM J Sci and Stat Comput 29(6):2283–2304 (electronic), DOI 10.1137/060660709, URL http://dx.doi.org/10.1137/060660709

Yuan J, Steidl G, Schnörr C (2008) Convex Hodge decomposition of image flows. In: Pattern recognition, Lecture Notes in Comput. Sci., vol 5096, Springer, Berlin, pp 416–425, DOI 10.1007/978-3-540-69321-5_42, URL http://dx.doi.org/10.1007/978-3-540-69321-5_42

Yuan J, Schnörr C, Steidl G (2009) Convex Hodge decomposition and regularization of image flows. J Math Imaging Vision 33(2):169–177, DOI 10.1007/s10851-008-0122-1, URL http://dx.doi.org/10.1007/s10851-008-0122-1